

## Inelastic scattering of 65 MeV protons from $^{12}\text{C}$ , $^{24}\text{Mg}$ , $^{28}\text{Si}$ , and $^{32}\text{S}$

S. Kato and K. Okada

*Laboratory of Nuclear Studies, Faculty of Science, Osaka University, Toyonaka, Osaka 560, Japan*

M. Kondo, K. Hosono, T. Saito, N. Matsuoka, K. Hatanaka, T. Noro, and S. Nagamachi

*Research Center for Nuclear Physics, Osaka University, Ibaraki, Osaka 567, Japan*

H. Shimizu

*Department of Physics, Faculty of Science, Kyoto University, Kyoto 606, Japan*

K. Ogino and Y. Kadota

*Department of Nuclear Engineering, Kyoto University, Kyoto 606, Japan*

S. Matsuki

*Institute for Chemical Research, Kyoto University, Kyoto 606, Japan*

M. Wakai

*Department of Physics, Faculty of Science, Osaka University, Toyonaka, Osaka 560, Japan*

(Received 21 November 1983; revised manuscript received 6 August 1984)

Measurements of angular distributions of the cross sections and analyzing powers for the elastic and inelastic scatterings of 65 MeV polarized protons from  $^{12}\text{C}$ ,  $^{24}\text{Mg}$ ,  $^{28}\text{Si}$ , and  $^{32}\text{S}$  are reported. Coupled channels analyses of the scattering data are presented assuming the  $0_1^+$ ,  $2_1^+$ , and  $4_1^+$  states to be members of the ground band, the  $0_2^+$  state to begin the  $\beta$  band, and the  $3_1^-$  state to begin the  $K^\pi=3^-$  band in  $^{12}\text{C}$ ; the  $0_1^+$ ,  $2_1^+$ , and  $4_1^+$  states to comprise the ground band, the  $2_2^+$ ,  $3_1^+$ , and  $4_2^+$  states to comprise the  $\gamma$  band, the  $3_1^-$  state to begin the  $K^\pi=3^-$  band, and the  $1_1^-$  and  $3_2^-$  states to comprise the  $k^\pi=0^-$  band in  $^{24}\text{Mg}$ ; and the  $0_1^+$ ,  $2_1^+$ , and  $4_1^+$  states to comprise the ground band, the  $0_2^+$  state to begin the  $\beta$  band, the  $3_1^-$ ,  $4_1^-$ ,  $5_1^-$ , and  $6_1^-$  states to comprise the  $k^\pi=3^-$  band, and the  $1_1^-$  and  $3_1^-$  states to comprise the  $K^\pi=0^-$  band in  $^{28}\text{Si}$ . The fit of the analyzing power of the  $\beta$  band  $0_2^+$  level is improved by mixing the breathing mode of oscillation into the  $\beta$  vibration. Coupled channels analyses of the experimental angular distributions are presented for the levels in  $^{32}\text{S}$  in which the  $0_1^+$ ,  $2_1^+$ , and  $4_1^+$  states were assumed to belong to the ground band, the  $0_2^+$  and  $2_3^+$  states to the  $\beta$  band, the  $2_2^+$ ,  $3_1^+$ , and  $4_2^+$  states to the  $\gamma$  band, the  $3_1^-$  state to the  $3^-$  band, and the  $1_1^-$  state to the  $0^-$  band. These states were treated assuming a symmetric rotator model. The coupled channels calculations in terms of a vibrational model were also performed for  $^{32}\text{S}$ . Multipole moments obtained from present data are compared to the moments deduced from hadron scattering and electromagnetic measurements. Transition strengths deduced from the (p,p') scattering are compared with gamma-ray decay widths for  $2^+$  states in the ground bands.

### I. INTRODUCTION

For the inelastic scattering of protons on light even-even nuclei with mass numbers of less than 30, macroscopic description has often been applied with fairly good success. Among these nuclei,  $^{24}\text{Mg}$  and  $^{28}\text{Si}$  have been extensively studied by inelastic scattering of protons.<sup>1-9</sup> These nuclei have been believed to have a substantial quadrupole deformation in their ground state. Their level structure shows the rotational structure characteristics of deformed nuclei. Many rotational bands were identified for  $^{24}\text{Mg}$ , i.e., the ground  $K^\pi=0^+$  band, the excited  $K^\pi=2^+$  band starting with the  $2_2^+$  state at 4.24 MeV which was identified as the  $\gamma$ -vibrational band, and the excited  $K^\pi=0^+$  band starting with the  $0_2^+$  state at 6.43 MeV which was thought to be a  $\beta$ -vibrational band. An

octupole  $K^\pi=0^-$  vibrational band starting from a  $1^-$  state at 7.55 MeV and an octupole  $3^-$  vibrational band starting at 7.62 MeV were also proposed.<sup>10</sup>

For the  $^{28}\text{Si}$  nucleus, besides the ground band, the  $K^\pi=0^+$  band starting from the  $0_2^+$  state at 4.98 MeV has been proposed to comprise the  $\beta$  band. The band starting with the  $3^-$  state at 6.88 MeV may be considered as an octupole band which contains the  $4^-$  (8.41 MeV),  $5^-$  (9.70 MeV), and  $6^-$  (11.58 MeV) levels. The band beginning with the  $1^-$  level at 8.90 MeV was thought to be a  $K^\pi=0^-$  octupole band.<sup>11</sup> The  $^{12}\text{C}$  nucleus is thought to be an oblately deformed nucleus in which a ground band, a  $\beta$ -vibrational state  $0^+$  at 7.65 MeV, and an octupole vibrational  $3^-$  state at 9.64 MeV has been considered.<sup>14</sup> These band structures are illustrated in Fig. 1. The  $^{32}\text{S}$  nucleus was usually thought to be spherical from the level

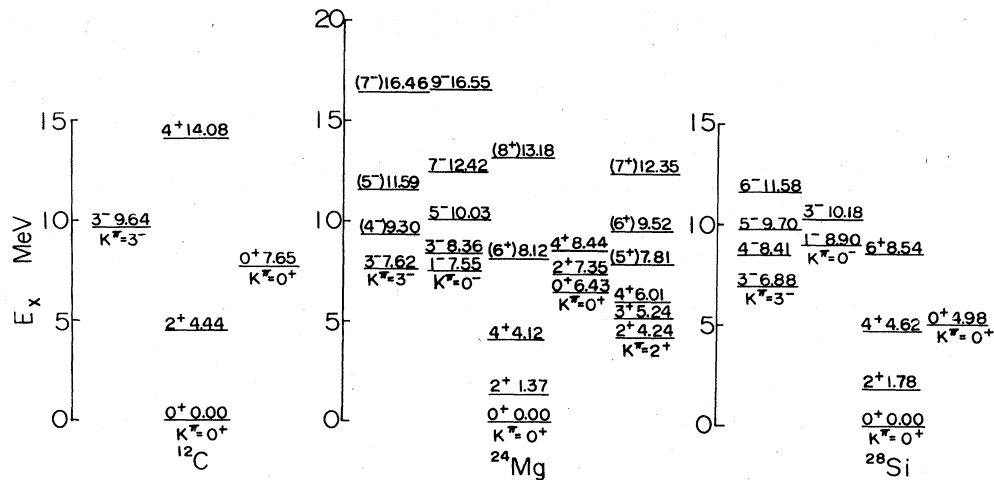


FIG. 1. Level structures of deformed nuclei  $^{12}\text{C}$ ,  $^{24}\text{Mg}$ , and  $^{28}\text{Si}$ . The levels are classified in a ground band, a  $\beta$  band, a  $\gamma$  band, and octupole vibrational bands.

structure but also it was assumed to be deformed.<sup>8</sup> In the latter assumption, the ground band, the  $\beta$ -vibrational state  $0^+$ , 3.78 MeV, the  $\gamma$  band starting with the  $2_2^+$ , 4.82 MeV, the octupole  $K^\pi=3^-$  band starting with the  $3^-$ , 5.01 MeV state, and the  $1^-$ , 5.80 MeV state, the head of a  $K^\pi=0^-$  octupole band, have been identified.

Inelastic scattering of protons on these levels has been analyzed by collective and microscopic shell models. Coupled channels (CC) analyses of the inelastic scattering of protons from light  $s$ - $d$  shell nuclei have been shown to be successful in providing the deformation parameters for the ground and  $\gamma$  bands.<sup>8,13</sup> However, there have been only a few CC analyses with both cross section and analyzing power data for the levels which belong to these bands. For  $0^+$  levels of the  $\beta$ -band head, several authors reported the importance of a mixing of a breathing oscillation into the  $\beta$  vibration from CC analyses of differential cross sections of  $(p,p')$  or  $(\alpha,\alpha')$  scattering.<sup>15,16</sup> We intended to elucidate the contribution of the breathing mode to the scattering using the analyzing power data as well as data of the differential cross sections.

We report here data of differential cross sections and analyzing powers of  $(p,p')$  scattering on  $^{12}\text{C}$ ,  $^{24}\text{Mg}$ ,  $^{28}\text{Si}$ , and  $^{32}\text{S}$  at 65 MeV with CC calculations to obtain more information on the levels belonging to the collective bands. The final states excited in the present experiment include the ground band,  $\beta$  and  $\gamma$  bands, and  $3^-$  and  $0^-$  octupole bands for  $^{24}\text{Mg}$ ; the ground band, the  $\beta$  band, and  $3^-$  and  $0^-$  octupole bands for  $^{28}\text{Si}$ ; the ground band, the  $0^+$  (7.65 MeV) and  $3^-$  (9.64 MeV) states for  $^{12}\text{C}$ ; and  $2^+$  (5.55),  $1^-$  (5.80),  $4^+$  (6.41), and  $4^-$  (6.62) for  $^{32}\text{S}$ . Deformation parameters are determined from analysis of the data for the ground band. They are compared to the values obtained in preceding experiments of hadron inelastic scattering and from electron inelastic scattering.

The multipole moments of the deformed optical potential have been extracted and related to those of the matter density using Satchler's theorem.<sup>17</sup> The moments of matter distributions in  $^{24}\text{Mg}$ ,  $^{28}\text{Si}$ , and  $^{32}\text{S}$  are compared to

electromagnetic measurements of the charge density multipole moments. The extracted multipole moments are also compared with those obtained in other analyses of inelastic scattering of hadrons, namely  $(p,p')$ ,  $(d,d')$ ,  $(^3\text{He},^3\text{He}')$ , and  $(\alpha,\alpha')$  scattering. Transition strengths between the  $2_1^+$  states and the ground states were deduced and compared with the corresponding widths of gamma-ray transitions.

Experimental details and results are described in Sec. II; the fits by coupled-channel Born approximation (CCBA) calculations are presented in Sec. III. Discussions are stated in Sec. IV. The summary and conclusions are finally given in Sec. V.

## II. EXPERIMENTAL METHODS AND RESULTS

The experiment was carried out using a polarized proton beam of 65 MeV energy from the AVF cyclotron of the Research Center for Nuclear Physics (RCNP), Osaka University. Polarized protons were produced by an atomic beam-type ion source.

For the levels in  $^{12}\text{C}$  and  $^{28}\text{Si}$  and low lying levels in  $^{24}\text{Mg}$ , emitted protons were detected by counter telescopes. A  $1.5 \text{ mg/cm}^2$   $^{24}\text{Mg}$  target whose isotopical enrichment was 99% was commercially obtained. A  $2.0 \text{ mg/cm}^2$   $^{28}\text{Si}$  target was fabricated by an etching technique using a natural silicon plate. Both thicknesses were measured by the energy loss of  $\alpha$  particles emitted from  $^{241}\text{Am}$ . For carbon, a  $20 \mu\text{m}$  thick polyethylene foil was used. The direction of the beam polarization was alternated at every  $0.2 \mu\text{C}$  of beam charge by changing the magnetic field of the ionizer of the polarized ion source.<sup>18</sup> After passing through the target, the beam was again focused onto a carbon polarimeter which monitored the beam polarization continuously during measurements. A beam polarization of 60–70% was routinely obtained with beam current up to 50 nA on the target.

The details of the experimental arrangement and procedures have been reported elsewhere.<sup>19</sup> The counter tele-

scope consisted of a  $\Delta E$  (700  $\mu\text{m}$  Si SSD) and an  $E$  (15 mm high purity Ge SSD cooled by liquid nitrogen) (SSD denotes solid state detector) detectors.<sup>20</sup> They were placed at symmetrical angles to the beam. The overall energy resolution including an energy spread of the incident beam, an energy broadening in the target, kinematical broadening, and intrinsic resolution of the detector ranged between 200 and 230 keV (FWHM). Protons were identified by a particle identification circuit. The analyzing powers were determined using four counts  $N_{LU}$ ,  $N_{LD}$ ,  $N_{RU}$ , and  $N_{RD}$  where L or R refers to the detector at left or right side of the beam axis and U or D refers to up or down of the polarization direction of the incident beam, respectively. Figure 2 displays a sample spectrum of  $^{24}\text{Mg}(p,p')$  scattering taken by the counter telescope of 30°. The  $^{12}\text{C}(p,p')$  spectrum is displayed in Ref. 21.

Scattered protons from  $^{32}\text{S}$  and some closely spaced levels of  $^{24}\text{Mg}$  were analyzed by means of a magnetic spectrograph RAIDEN.<sup>22</sup> In this measurement, the beam was analyzed to reduce the energy spread, and overall energy resolution was 50 keV. The ionizer of the polarized ion source yielded an analyzed beam intensity of typically 30 nA. The beam intensity was reduced to 5 or 10 nA to reduce the target evaporation for the sulphur target. The target, 3 mg/cm<sup>2</sup> thick, was fabricated by vacuum evaporation of natural sulphur powder on a Au foil of thickness 1.7 mg/cm<sup>2</sup>. The background due to the Au foil was measured using it as a target and ascertained to be negligibly small. The sign of the beam polarization was alternated using the high and low field rf transitions between Zeeman levels of atomic hydrogen.<sup>23</sup> Figure 3 displays the experimental setup schematically. The polarimeter target on the beam line was stepped aside from the beam line for ninety seconds while a spectrum was taken with the spectrograph after measurement for ten seconds. The protons were detected by a 1.5 m focal plane detector.<sup>24</sup> The detector consisted of a position sensitive resistive-wire proportional counter followed by proportional counters

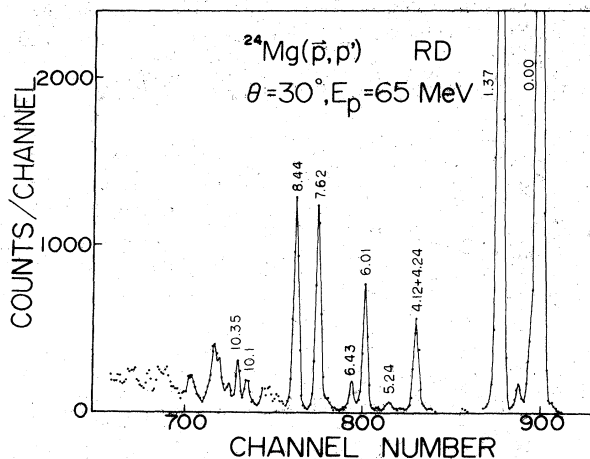


FIG. 2. Pulse height spectrum, employing a counter telescope, of  $^{24}\text{Mg}(p,p')$  scattering taken at 30° laboratory angle and at an incident energy of 65 MeV. RD means the spectrum taken at right side to the incident beam with spin down direction.

( $\Delta E_1$  and  $\Delta E_2$ ) and a plastic  $E$  counter. They were operated in a fourfold coincidence mode. The particle identification was performed by using the  $E_1$ ,  $E_2$ , and  $E$  signals. Since the range of energy acceptance in RAIDEN is about 3 MeV at 60 MeV with the 1.5 meter counter, the first series of the measurement contained only the ground and the first excited states, the second series covered from the first excited state to 5.5 MeV excitation, and the third series covered the levels at higher excitation energy containing the 3<sup>-</sup> state. The spectrum of each series was taken by changing the magnetic field of RAIDEN. Absolute values of the cross sections of  $^{32}\text{S}(p,p')$  scattering were determined by normalizing present data to those taken by Nakamura *et al.*<sup>25</sup> who used sulphur hydride gas as a target. Figure 4 is a momentum spectrum of protons taken for  $^{32}\text{S}$  at 40° by the RAIDEN. The overall energy resolution was about 50 keV FWHM. The spread came mainly from energy loss in the target. A peak-fitting technique was applied to the closely spaced level pairs to obtain the yield of each level which could not clearly be separated from others in the spectrum. They were level pairs of (7.553, 7.616 MeV) and (8.358, 8.436 MeV) in  $^{24}\text{Mg}$ . An individual yield was extracted assuming the same shape of each level with a single well-known level. The analyzing powers were obtained from  $A_y = (1/P)(N_U - N_D)/(N_U + N_D)$ , where  $N_U$  ( $N_D$ ) is the count taken at the left side angle to the incident beam with up (down) spin direction and  $P$  is the incident beam polarization determined by the polarimeter. The statistical errors of the cross sections did not exceed 3% in most levels. At very forward angles, the error caused from the background subtraction was dominant. The absolute normalization of all cross section data is accurate to  $\pm 10\%$ . The final errors of the analyzing powers were assumed to be statistical.

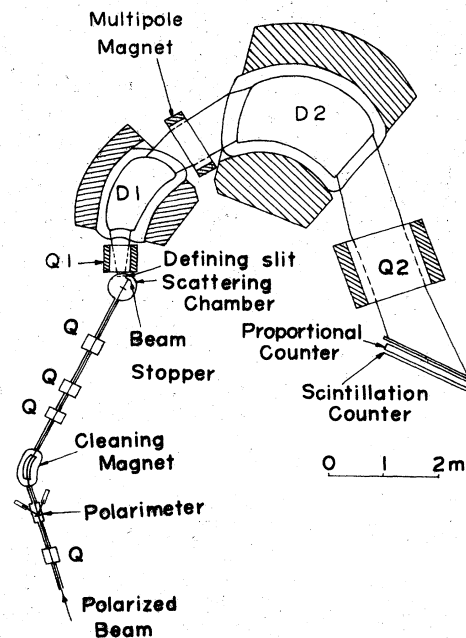


FIG. 3. Schematic plan view of the experimental setup with the magnetic spectrograph RAIDEN.

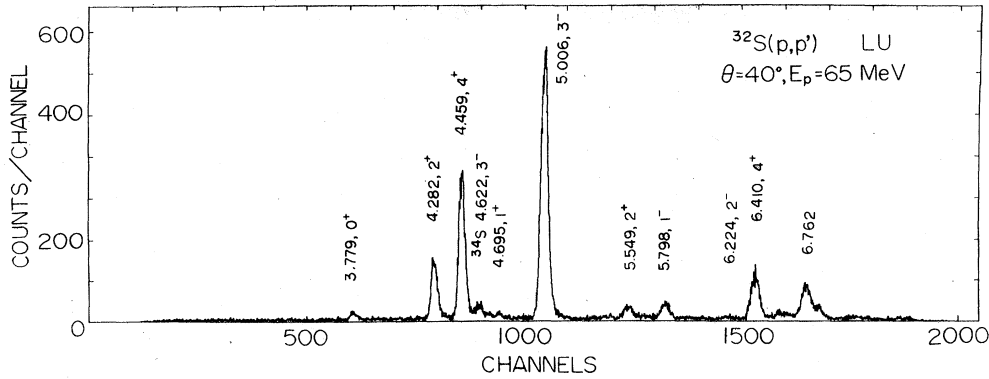


FIG. 4. Energy spectrum of  $^{32}\text{S}(p,p')$  scattering at  $40^\circ$  laboratory angle. The spectrum was taken by the magnetic spectrograph RAIDEN. See also the caption of Fig. 2.

### III. COUPLED CHANNELS ANALYSIS

In this section, the results of CC calculations on the  $^{12}\text{C}$ ,  $^{24}\text{Mg}$ ,  $^{28}\text{Si}$ , and  $^{32}\text{S}(p,p')$  scattering are given. The CC calculations were done by using the code JUPITOR (Refs. 26 and 27) in a modified form in which an  $L$ - $S$  potential was included with the Oak-Ridge deformed form.<sup>28</sup> The optical potential is the usual Woods-Saxon form. In the rotational model of deformed nuclei, the radius parameter  $R(\theta')$  is angle dependent according to

$$R(\theta') = R_0 [1 + \beta_2 Y_{20}(\theta') + \beta_4 Y_{40}(\theta')] . \quad (1)$$

The optical potential parameters for protons on these nuclei were obtained by fitting the calculated elastic cross sections and polarizations to those measured in the present experiment by means of an automatic search code SEARCH (Ref. 29) or MAGALI (Ref. 30). The optical model fit to the experimental points is illustrated in Fig. 5. The parameters are listed in Table I. In the search procedure, the Coulomb radius parameter  $r_C$  was fixed at 1.30 or 1.25 fm.

The CC calculations assuming the rotational model of deformed nuclei were performed for  $^{12}\text{C}$ ,  $^{24}\text{Mg}$ ,  $^{28}\text{Si}$ , and  $^{32}\text{S}$ . A CC calculation of the vibrational model of spherical nuclei was also performed for  $^{32}\text{S}$ . In the calculations assuming deformed nuclei, both nuclear and Coulomb potentials were deformed. The same deformation parameters were used for all potential terms. The axially symmetric rotational model with quadrupole and hexadecapole deformations was used to describe the ground state band. The  $\gamma$ -band states were assumed to correspond to a

$\gamma$  vibration in which the nucleus retained the same equilibrium and spheroidal deformation, but in addition oscillates such that ellipsoidal shapes were produced ( $K^\pi = 2^+$  band). The  $\beta$ -band states were thought to correspond to  $\beta$  vibration in which the nucleus oscillated about a given equilibrium deformation, always retaining its axial symmetry ( $K = 0^+$  band).<sup>31</sup>

For the excitation of states belonging to the vibrational band of even, deformed nuclei, Eq. (1) is extended as

$$R(\theta) = R_0 \left[ 1 + \sum_{\lambda} \beta_{\lambda} Y_{\lambda 0}(\theta') + \sum_{i=1}^2 \alpha_{\lambda_i 0} Y_{\lambda_i 0}(\theta') + \sum_{i=3}^6 \frac{1}{\sqrt{2}} (\alpha_{\lambda_i K_i} Y_{\lambda_i K_i}(\theta') + \alpha_{\lambda_i -K_i} Y_{\lambda_i -K_i}(\theta')) \right] , \quad (2)$$

where  $i = 1, 2, 3, 4, 5$ , and  $6$  stand for  $K^\pi = 0^+, 0^-, 2^+, 1^-, 2^-$ , and  $3^-$  vibrations, respectively.<sup>27</sup> The  $\alpha_{\lambda_i K_i}$  are operators which are equal to a linear combination of creation and annihilation operators of the phonons corresponding to the various vibrations; for example,  $K^\pi = 0^+$ , and  $\alpha_{20}$  means  $\beta$ - $\beta_2$ . We included only  $\alpha_{22}(Y_{22} + Y_{2-2})$  terms which directly excite only the  $2^+$  member of the  $\gamma$  band. We did not take into account an additional  $\alpha_{42}(Y_{42} + Y_{4-2})$  coupling which permitted direct transition from the ground state to the  $4^+$  member of the  $\gamma$  band. The  $\beta_{\lambda}$  are deformation of  $2^\lambda$ -pole shape. We defined quantities  $\eta_i$  as<sup>27</sup>

TABLE I. Optical parameters for 65 MeV protons.

	$V$	$r_R$	$a_R$	$W_V$	$W_S$	$r_I$	$a_I$	$V_{SO}$	$r_{SO}$	$a_{SO}$	$r_C$
	(MeV)	(fm)	(fm)	(MeV)	(MeV)	(fm)	(fm)	(MeV)	(fm)	(fm)	(fm)
$^{12}\text{C} + p$	25.39	1.244	0.714	5.16	0.00	1.469	0.39	6.79	1.041	0.620	1.30
$^{24}\text{Mg} + p$	37.84	1.14	0.722	8.04	1.65	1.390	0.542	5.52	1.000	0.621	1.25
$^{28}\text{Si} + p$	38.61	1.13	0.749	7.63	2.05	1.365	0.482	5.50	1.020	0.595	1.25
$^{32}\text{S} + p$	30.51	1.20	0.827	3.84	2.08	1.36	0.67	3.66	1.01	0.59	1.25

$$\begin{aligned} \eta_i &= \langle \text{ground state} | \alpha_{\lambda,0} | \text{vibrational state} \rangle \text{ for } i=1,2, \\ &= \sqrt{2} \langle \text{ground state} | \alpha_{\lambda,K_i} | \text{vibrational state} \rangle \text{ for } i=3,4,5,6. \end{aligned} \quad (3)$$

The definition is the same as that of Ref. 6. The parameter  $\eta_i$  corresponds to the coupling parameter of the excitation of the vibrational state.

We calculated the angular distributions of the  $\beta$ -band levels taking into account the mixing of the breathing mode into the  $\beta$  vibration to make clear the contribution of it in the analyzing power. We assumed a simple radial scaling of the nuclear density distribution with  $r'=r(1-\alpha)$ .<sup>32</sup> Upon quantization, the deformation parameter  $\alpha$  was thought to be an operator. The central part of the optical potential was deformed in the same way as the density. An additional term to the central optical potential  $V_{\text{central}}$  was

$$-\frac{\alpha}{r^2} \frac{d}{dr} (r^3 V_{\text{central}}).$$

With the inclusion of the breathing mode into the  $\beta$  vibration, an additional term also arose in the spin-orbit part. The term is

$$-\alpha V_{LS} \left[ \frac{\hbar}{m_{\pi} c} \right]^2 \left[ \frac{4}{r} \frac{df}{dr} + \frac{d^2 f}{dr^2} \right] L \cdot S,$$

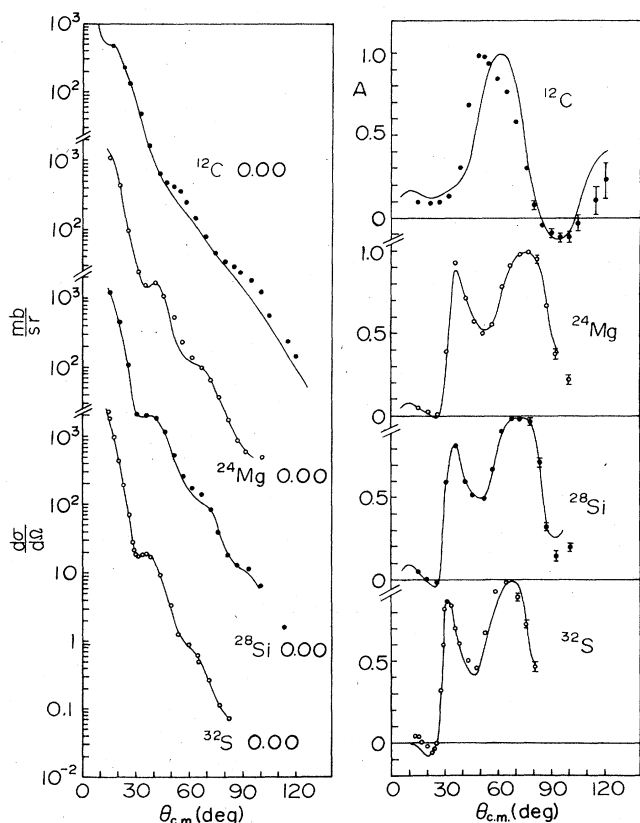


FIG. 5. Angular distributions of the cross sections and analyzing powers of elastic scattering from the four isotopes of interest. Curves are optical model fits to the data.

where  $f$  means the usual Woods-Saxon function. We took the same geometrical parameters for the additional  $L$ - $S$  term as the original  $L$ - $S$  term. The value of the matrix element

$$\eta = \sqrt{4\pi} \langle \text{ground state} | \alpha | \beta\text{-vibrational state} \rangle \quad (4)$$

should be determined to give the best agreement between experimental and theoretical results.

### A. $^{12}\text{C}$

In the CC calculations,  $^{12}\text{C}$  was assumed to be deformed with coupling of the  $0^+$ ,  $2^+$ , and  $4^+$  states assuming the strict rotational model. The results of CC calculations for the  $0^+$ ,  $2^+$ , and  $4^+$  states of the ground band are shown in Fig. 6. The deformation parameters for curves in the figure are  $\beta_2 R = -1.82$ ,  $\beta_4 R = +0.17$  fm, where  $R = r_R A^{1/3}$  and  $r_R$  is the radius parameter of the real optical potential. The fit between the data and the calculation with the positive value of  $\beta_2$  is worse than that with the negative value of  $\beta_2$ . The result of an oblate shape of

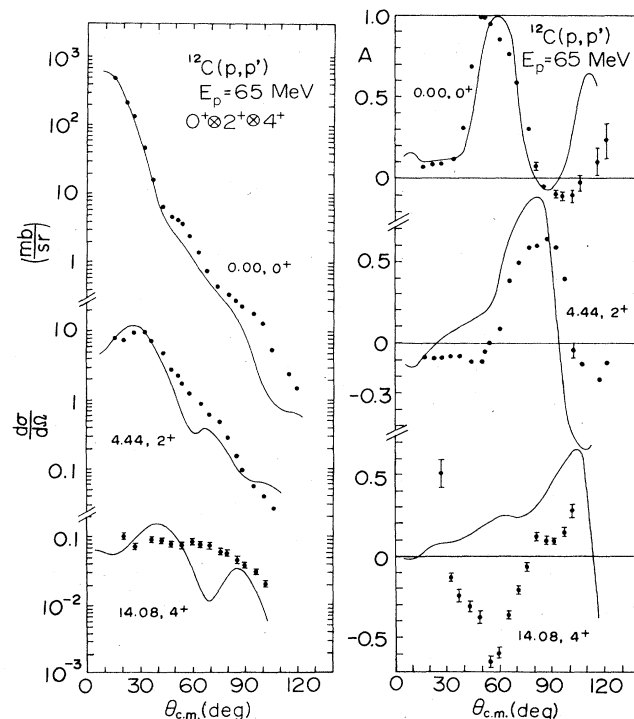


FIG. 6. Experimental angular distributions of the cross sections and analyzing powers and CC calculations for inelastic proton scattering on  $^{12}\text{C}$  exciting the ( $0^+$ , 0.00), ( $2^+$ , 4.44), and ( $4^+$ , 14.08 MeV) states. These states are assumed to belong to the ground state rotational band. The deformation lengths are  $\beta_2 R = -1.82$  fm and  $\beta_4 R = 0.17$  fm where  $R = r_R A^{1/3}$ . In the CC calculations the axially symmetric deformed rotational model is used.

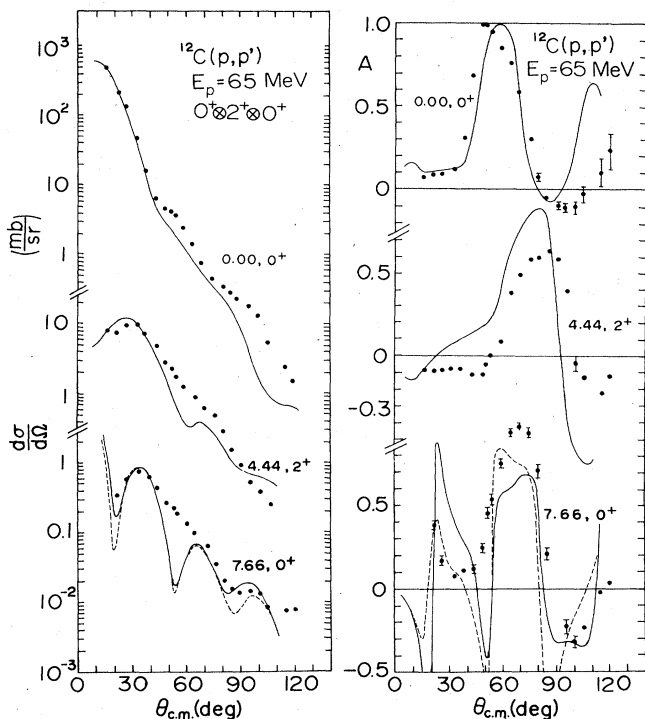


FIG. 7. Same as Fig. 6 except the 7.65 MeV state is taken to belong to the  $\beta$  band with  $\eta_{\beta}R = 1.48$  fm. The dashed curves are the results which include the effect of breathing oscillation with amplitude parameter  $\eta = -0.2$ . Accordingly the value of  $\eta_{\beta}R$  is reduced to 1.14 fm.

the  $^{12}\text{C}$  nucleus is consistent with the result obtained by electron scattering<sup>34</sup> and also by proton scattering at 800 MeV.<sup>14</sup> Although the strength is roughly correct, the fit to the data is unsatisfactory for the  $4^+$ , 14.08 MeV state in both the cross section and analyzing power.

In Fig. 7 a comparison between the data and the CC results is shown for the 7.66 MeV,  $0^+$  state which is assumed to be a  $\beta$ -vibrational state. The comparison was done in order to investigate whether the  $0^+$  state can be described possibly as the head of a  $\beta$ -vibrational band. All states in the figure are coupled. The coupling parameter of the  $\beta$  vibration is determined to be 0.52 from the cross section data. The value corresponds to a coupling length  $\eta_{\beta}R = 1.48$  fm. The fit to the data is fair, especially for the analyzing power. The CC prediction by means of the positive value of  $\beta_2$  gave a worse fit to the data compared with that of negative value for the level. Calculated curves including the breathing oscillation in the  $\beta$  vibration are drawn by dashed curves which show some improvement of the fit to the analyzing power data. The value  $\eta_{\beta}R$  is reduced to 1.14 fm corresponding to  $\eta = -0.2$ , the breathing mode matrix element (4). A positive value of the  $\eta$  is not suitable in obtaining a good fit to the analyzing power.

In Fig. 8 the comparison of the data and the calculation is shown for the 9.64 MeV,  $3^-$  state where the hexadecapole deformation is not taken into account. A coupling parameter  $\eta_3 = 0.33$  ( $\eta_3R = 0.94$  fm) was determined to fit

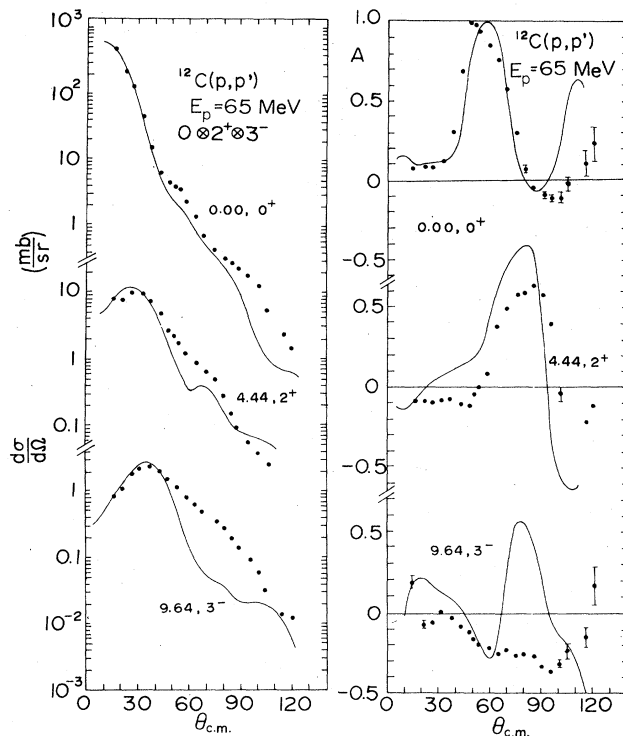


FIG. 8. Same as Fig. 6 except the 9.64 MeV state is taken to belong to the  $3^-$  octupole band with  $\eta_3R = 0.94$  fm.

the CC curve to that of the cross section data. The fit between data and calculations for  $3^-$  levels is quite unsatisfactory, especially for the analyzing power.

### B. $^{24}\text{Mg}$

Calculations for the  $(0.00, 0^+)$ ,  $(1.37, 2^+)$ , and  $(4.12, 4^+)$  states were made assuming them to be members of the ground state rotational band as shown in Fig. 1. The quadrupole and hexadecapole deformations were taken into account. The  $\beta_2 = +0.48$  was determined to fit the cross section data of the  $2^+$  state and  $\beta_4 = -0.02$  was adjusted to reproduce the  $4^+$  state cross section. The comparison is illustrated in Fig. 9 while the corresponding values of deformation lengths  $\beta_2R = 1.58$  fm and  $\beta_4R = -0.07$  fm. The CC curve is a factor of 2 below the first maximum in the  $A_y$  angular distribution for the  $2_1^+$  state. This came from the adoption of the simplified form of the deformed  $L$ - $S$  potential<sup>28</sup> instead of the full Thomas  $L$ - $S$  potential.<sup>33</sup> The fit to the  $4^+$  level is rather unsatisfactory, especially for analyzing power. This is in contrast to the result of 800 MeV incident energy<sup>13</sup> where the cross section is reproduced well by the CC calculation.

In Fig. 10, the results for the  $\gamma$  band of  $^{24}\text{Mg}$  are given. For the calculations the  $(4.24, 2^+)$ ,  $(5.24, 3^+)$ , and  $(6.01, 4^+)$  states were considered to be members of the band. The experimental angular distributions for ground band  $2^+$  and the  $\gamma$  band  $2^+$  are very similar. The CC curves for these  $2^+$  levels resemble and fit the data well. The coupling parameter for the  $\gamma$ -vibrational band was determined to be  $\eta_{\gamma} = 0.17$  and  $\eta_{\gamma}R = 0.56$  fm using the above

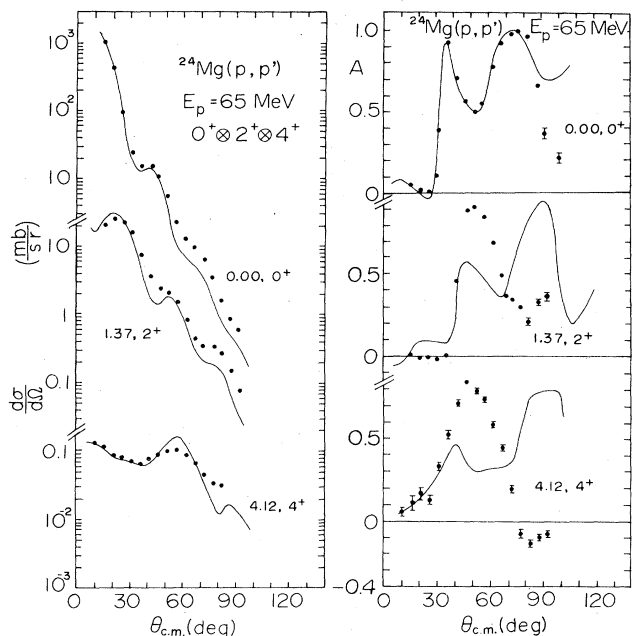


FIG. 9. Experimental angular distributions of the cross sections and analyzing powers and CC calculations for inelastic proton scattering on  $^{24}\text{Mg}$  exciting the ground state band ( $0^+$ ,  $0.00$ ;  $2^+$ ,  $1.37$ ; and  $4^+$ ,  $4.12$  MeV) in which all states are coupled. The coupling lengths are  $\beta_2 R = 1.58$  fm and  $\beta_4 R = -0.07$  fm, where  $R = r_R A^{1/3}$ . In the CC calculations the axially symmetric deformed rotational model is used.

determined  $\eta_2 = 0.48$ . The agreement between the data and CC prediction is fair for both cross section and analyzing power for the  $2^+$  state of the band head. However, the CC calculation could not produce the magnitude of the cross sections for  $3^+$  and  $4^+$  states of the band.

The ( $6.43$ ,  $0^+$ ), ( $7.35$ ,  $2^+$ ), and ( $8.44$ ,  $4^+$ ) states were assumed to be members of the  $\beta$ -vibrational band in  $^{24}\text{Mg}$  in the CC calculations. The results are compared with the data in Fig. 11. The coupling parameter was determined to be  $\eta_\beta = 0.18$ ,  $\eta_\beta R = 0.59$  fm to reproduce roughly the magnitude of the cross section of the  $0^+$  state. However, this value has some ambiguity which comes from the lack of the data around  $30^\circ$ . The agreement between the data and the CC results is good for the analyzing power of the  $0^+$  level, while the fit is poor for the cross section. The quality of the fit of the  $7.35$ ,  $2^+$  level is worse compared to that given for the  $0^+$  state. Dashed curves are CC calculations in which the breathing oscillation is added to the  $\beta$  vibration. The amplitude parameter  $\eta$  of the breathing oscillation in Eq. (4) is taken to be  $0.05$  and the value  $\eta_\beta R$  is maintained to be the same as above. A deep dip at  $15^\circ$  in the curve of the analyzing power of the  $0^+$  level is raised toward the data by the addition of the breathing oscillation. Effects of the additional mode to the  $2^+$  and  $4^+$  states should be small.

Data for the excitation of the ( $7.62$ ,  $3^-$ ) state in  $^{24}\text{Mg}$  are presented in Fig. 12. The curves in the figure are the CC calculation assuming an octupole  $K^\pi = 3^-$  vibration to this state. The coupling parameter is deduced to be

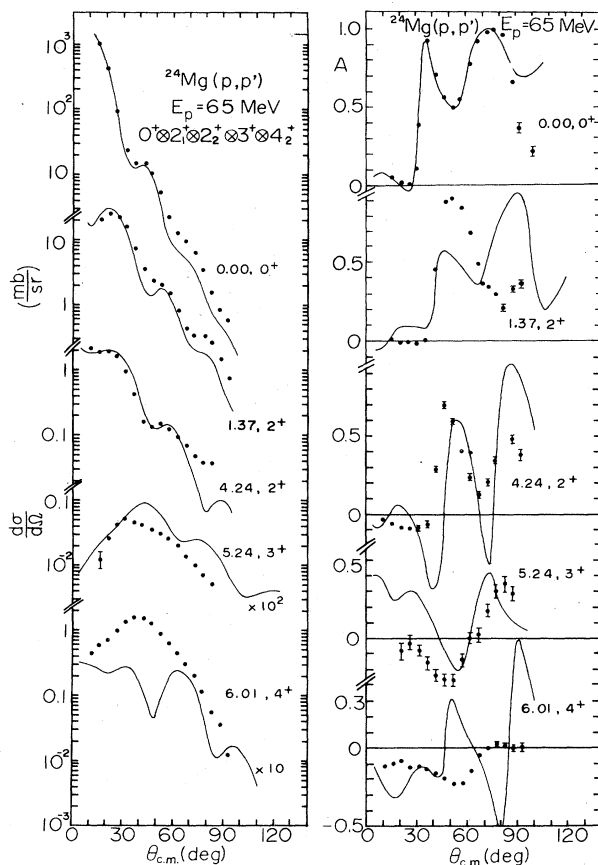


FIG. 10. Same as Fig. 9 except the  $4.24$ ,  $2^+$ ;  $5.24$ ,  $3^+$ ; and  $6.01$ ,  $4^+$  states are assumed to belong to the  $\gamma$  band and  $\eta_\gamma R = 0.56$  fm.

$\eta_3 = 0.3$  and  $\eta_3 R = 0.86$  fm. The fit to the  $3^-$  state is rather satisfactory, especially for the analyzing power.

The CC fits to the data of the excitation of the ( $7.55$ ,  $1^-$ ) and ( $8.35$ ,  $3^-$ ) states are presented in Fig. 13. They were assumed to belong to the octupole  $K^\pi = 0^-$  vibrational band. The coupling length is  $\eta_{0^-} R = 0.59$  fm. The fit is quite unsatisfactory for the  $1^-$  state.

### C. $^{28}\text{Si}$

The  $0^+$ ,  $0.00$ ;  $2^+$ ,  $1.78$ ; and  $4^+$ ,  $4.62$  MeV states were treated as members of the ground-state rotational band and couplings among all three states were taken into account. Since evidence for the oblate shape of the  $^{28}\text{Si}$  nucleus has been presented,<sup>31,32,35</sup> the coupling parameter  $\beta_2$  of the ground band was taken to be negative. The curves of CC predictions for this band are shown in Fig. 14, in which curves represent the CC results with  $\beta_2 R = -1.17$  fm and  $\beta_4 R = 0.45$  fm.

In Fig. 15 a comparison between the data and the CC predictions is illustrated for the  $0^+$ ,  $4.98$  MeV state. Angular shapes of the cross sections and analyzing powers are very similar to those of the  $0^+$ ,  $6.43$  MeV level of  $^{24}\text{Mg}$ . The coupling parameter  $\eta_\beta$  is derived to be  $0.23$  and  $\eta_\beta R = 0.79$  fm. The theoretical fit to the data is good

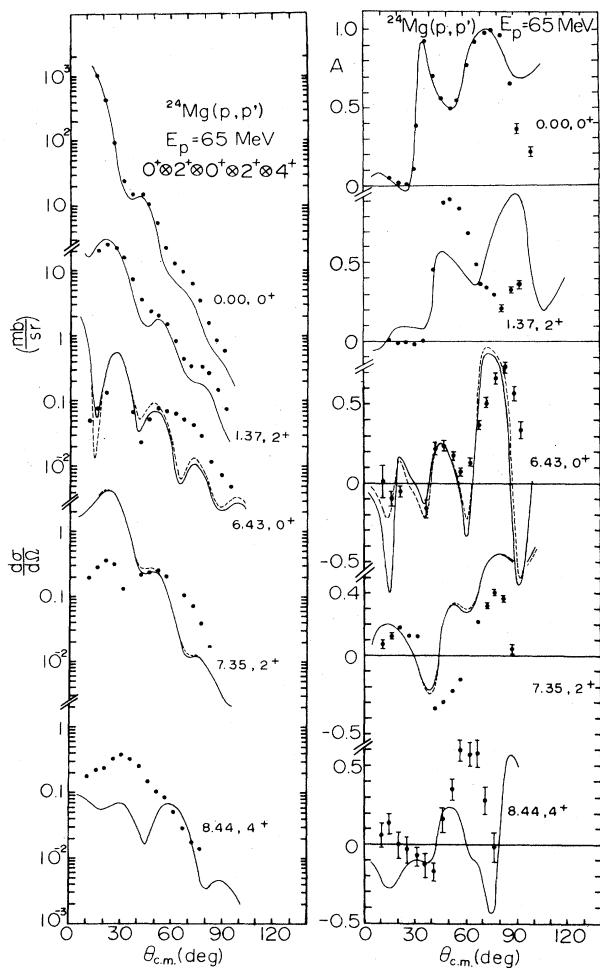


FIG. 11. Same as Fig. 9 except the  $6.43, 0^+$ ;  $7.35, 2^+$ ; and  $8.44, 4^+$  states are assumed to belong to the  $\beta$  band and  $\eta_{\beta}R = 0.59$  fm. The dashed curves are the results which include the effect of breathing oscillation with amplitude parameter  $\eta = 0.05$ . The value of  $\eta_{\beta}R$  is taken to be the same as above. The CC curves of higher members of the band are not affected appreciably by the breathing mode.

for analyzing power over the whole angular range compared, whereas the CC curve deviates from the data at angles larger than  $60^\circ$  for the cross section. Dashed curves are the CC curves which include the contribution of the breathing mode in the  $\beta$  vibration. The very deep dip at  $10^\circ$  in the analyzing power curve with  $\eta = 0$  is filled in by the inclusion of the mode. The value of  $\eta$  adopted is  $-0.1$ , and accordingly  $\eta_{\beta}R$  is reduced to  $0.72$  fm. A positive value of  $\eta$  is unsuitable to fit the data.

The levels  $6.88, 3^-$ ;  $8.41, 4^-$ ;  $9.70, 5^-$ , and  $11.58, 6^-$  are assumed to be members of an octupole  $3^-$  band. Their data are shown in Fig. 16 with CC curves. For the curves in Fig. 16, parameters  $\eta_3 = 0.22$  and  $\eta_3R = 0.78$  fm are used. They are determined by fitting the CC cross section of the  $3^-$  state to the data. The fit is not very satisfactory. For the  $4^-$  state the fit to the data is not satisfactory, with the CC cross section lower by a factor of  $\sim 3$ . The height of the peak around  $\theta \sim 60^\circ$  in the analyz-

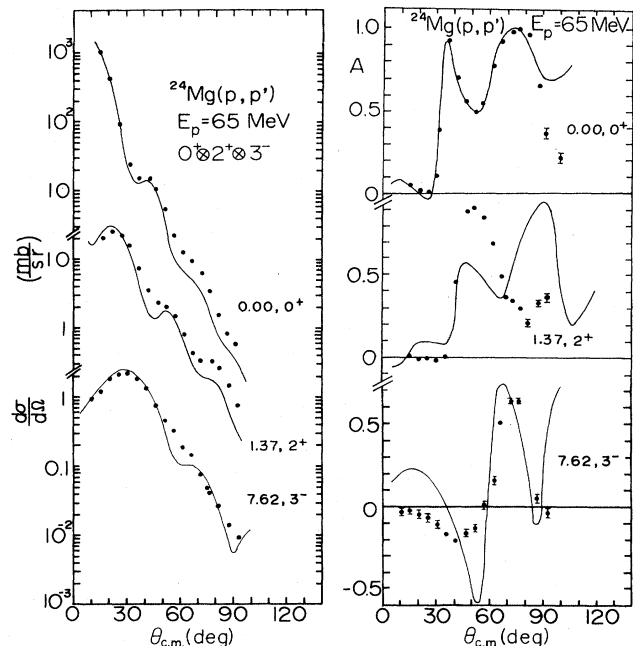


FIG. 12. Same as Fig. 9 except the  $7.62, 3^-$  state is assumed to belong to the octupole vibrational band and  $\eta_3R = 0.86$  fm.

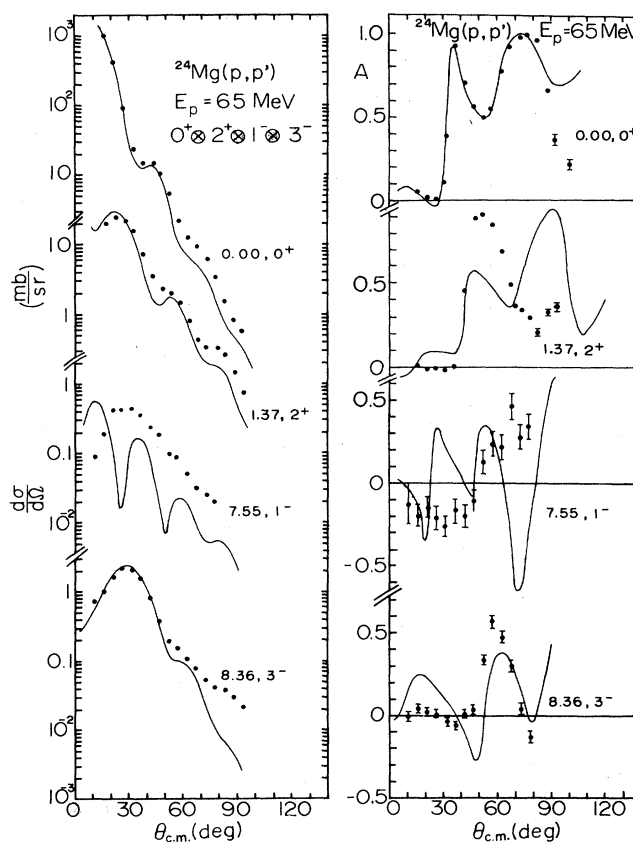


FIG. 13. Same as Fig. 15 except the  $7.55, 1^-$  and  $8.36, 3^-$  states are assumed to belong to the octupole  $K^\pi = 0^-$  band and  $\eta_{0-}R = 0.59$  fm.

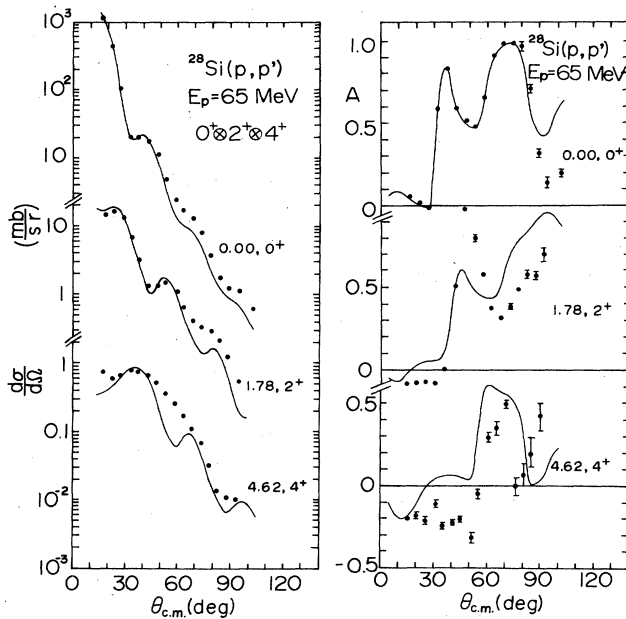


FIG. 14. Experimental angular distributions of the cross sections and analyzing powers and CC calculations for inelastic proton scattering on  $^{28}\text{Si}$  exciting the ground band ( $0^+$ , 0.00;  $2^+$ , 1.78; and  $4^+$ , 4.62 MeV) in which all states are coupled. The coupling parameters are  $\beta_2 R = -1.17$  fm and  $\beta_4 R = -0.45$  fm, where  $R = r_0 A^{1/3}$ . In the CC calculations the axially symmetric deformed rotational model is used.

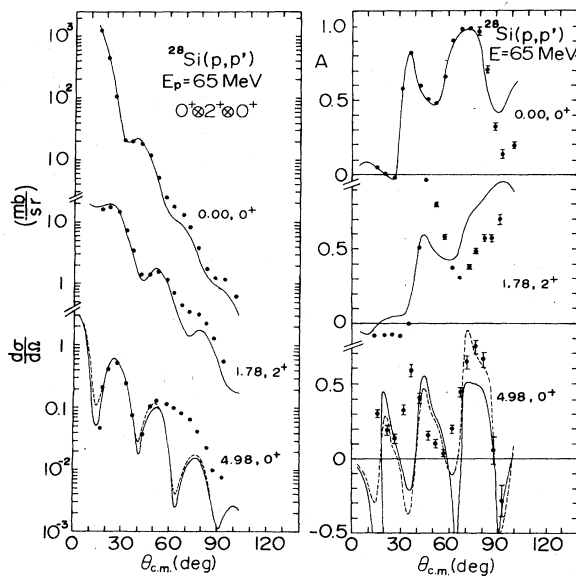


FIG. 15. Same as Fig. 14 except the 4.98 MeV,  $0^+$  state is assumed to belong to the  $\beta$  band and  $\eta_{\beta} R = 0.79$  fm. Dashed curves are the results which include the effect of a breathing oscillation with amplitude parameter  $\eta = -0.1$ . Accordingly the value of  $\eta_{\beta} R$  is reduced to 0.72 fm.

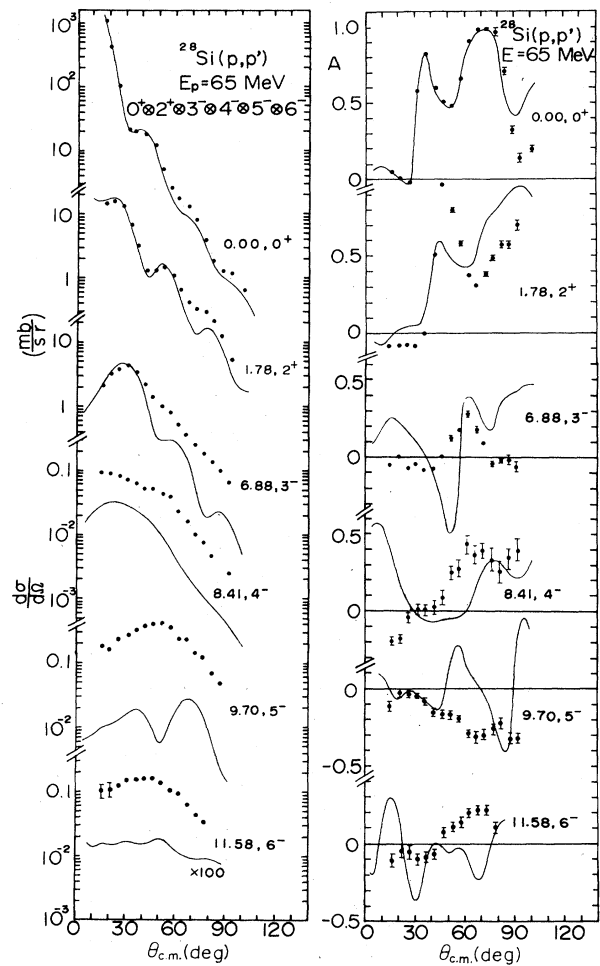


FIG. 16. Same as Fig. 14 except the 6.88,  $3^-$ ; 8.41,  $4^-$ ; 9.70,  $5^-$ ; and 11.58,  $6^-$  states are assumed to belong to the  $3^-$  octupole vibrational band and  $\eta_3 R = 0.75$  fm.

ing power of the  $3^-$  state is lower than that of the corresponding  $3^-$  state at 7.61 MeV in  $^{24}\text{Mg}$ . The CC calculation failed to produce the rather large cross section of higher members of the band, 9.70,  $5^-$  and 11.58,  $6^-$  levels, by factors of  $10^{-1}$  and  $10^{-3}$ , respectively.

The 8.90 MeV,  $1^-$  and 10.13 MeV,  $3^-$  states were assumed to be members of the octupole  $K^\pi = 0^-$  vibrational band in the calculations whose results are shown in Fig. 17. The coupling parameter  $\eta_0 = 0.143$  ( $\eta_0 R = 0.49$  fm) was determined to fit the CC curve to the experimental cross section of the 10.18 MeV state. The fit to the cross section is fair, but that to the analyzing power of the state is less satisfactory. The fit to the  $1^-$ , 8.90 state of the band head is quite unsatisfactory. The CC cross section is lower in magnitude and is out of phase with the data.

#### D. $^{32}\text{S}$

The  $^{32}\text{S}$  nucleus was at first assumed to be a deformed one in the CC calculations. From this point of view, the

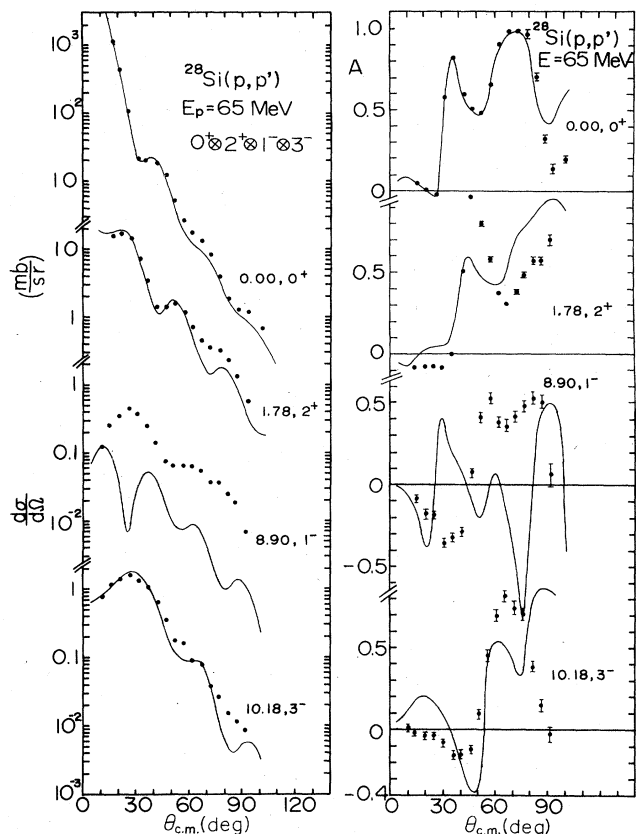


FIG. 17. Same as Fig. 14 except the 8.90,  $1^-$  and 10.18,  $3^-$  states are assumed to belong to the octupole  $K^\pi=0^-$  vibrational band and  $\eta_0 R=0.49$  fm.

level structure was decomposed as a ground rotational band, the  $\beta$  band  $0^+$  (3.78) and  $2^+$  (5.55), the  $\gamma$  band  $2^+$  (4.28),  $3^+$  (5.41), and  $4^+$  (6.42), the octupole band  $3^-$  (5.01) and  $4^-$  (7.95), and the octupole  $K^\pi=0^-$  band  $1^-$  (5.80) levels. Calculations for the ground band are given in Fig. 18, where deformation parameters  $\beta_2$  and  $\beta_4$  were taken into account. The deformation lengths  $\beta_2 R=0.84$  fm and  $\beta_4 R=-0.42$  fm were determined to fit the CC calculations to the cross section data for the  $2^+$  and  $4^+$  states.

In Fig. 19, a comparison between the CC predictions and the data is given for the  $\beta$ -band levels. Both the cross sections and analyzing powers cannot be reproduced by the calculations for the  $0^+$ , 3.78 MeV and the  $2^+$ , 5.55 MeV states. The data for the excitation of the  $2^+$  and  $4^+$  states assumed to belong to the  $\gamma$  band are illustrated in Fig. 20 with CC predictions. The value of  $\eta_\gamma R=0.48$  fm was found to reproduce the cross section of the  $2^+$  state. Both angular distributions of the  $2^+$  state are very similar to those of the  $2^+$  state in the ground rotational band. A  $3^+$ , 5.41 MeV level has too small a cross section to be obtained in this experiment.

A comparison of CC curves with the data for the octupole vibrational state at 5.01 MeV is given in Fig. 21. The theoretical fit to the data is excellent for the cross section,

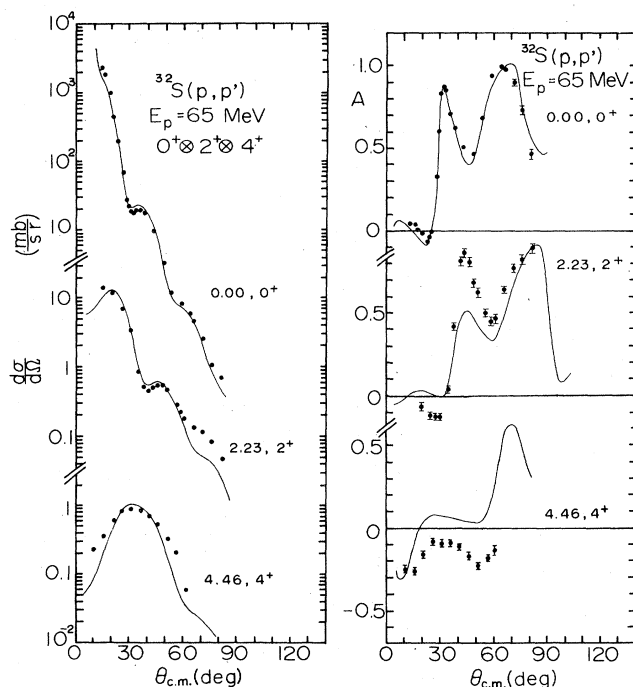


FIG. 18. Experimental angular distributions of the cross sections and analyzing powers and CC calculations for inelastic scattering on  $^{32}\text{S}$  which is assumed to be a deformed nucleus. This figure contains ground band states ( $0^+$ , 0.00;  $2^+$ , 2.23; and  $4^+$ , 4.62 MeV) in which all states are coupled. The coupling parameters are  $\beta_2 R=0.84$  fm and  $\beta_4 R=-0.42$  fm, where  $R=r_0 A^{1/3}$ . In the CC calculations the axially symmetric deformed rotational model is used.

while the fit to the analyzing power is rather poor. The deduced coupling length of the octupole vibrational state is  $\eta_3 R=1.05$  fm. A  $4^-$  level in this band was not detected in this measurement.

Experimental angular distributions for excitation of the  $1^-$ , 5.80 MeV state belonging to the octupole vibrational  $K^\pi=0^-$  band are given in Fig. 22. The  $\eta_0 R$  parameter tentatively used was 1.5 fm. The CC calculations are a poor representation of the data.

The nucleus  $^{32}\text{S}$  has been considered to be spherical from the level structure. The CC calculations assuming the vibrational model for  $^{32}\text{S}$  were also performed. In Fig. 23, a comparison between the CC predictions and the data is given for one quadrupole ( $2^+$ , 2.23) and two quadrupole ( $0^+$ , 3.78;  $2^+$ , 4.28; and  $4^+$ , 4.46) phonon states. The coupling constant between the ground and  $2_1^+$  states was taken to be  $\beta_{02}=0.24$ , one between the  $2_1^+$  state and two phonon  $0^+$ ,  $2^+$ , and  $4^+$  states to be  $\beta_{20}=\beta_{22}=\beta_{24}=0.24$ , direct coupling parameters between the ground and two phonon states to be  $\beta''_{00}=0.12$  (dashed curve) or  $-0.12$  (solid curve), and  $\beta''_{04}=0.12$  (dashed curve) or  $-0.12$  (solid curve). The sign of  $\beta''_{0I}$  ( $I=0, 2$ , and  $4$ ) came from the phase of the admixed one-phonon amplitude in the two-phonon states.<sup>37</sup> It is hard to say which sign is better to fit the calculation to the data. The  $\beta_{02}$  is just the  $\beta_2$  in Eq. (36.1) in Ref. 26 and  $\beta_{2I}$  is the  $\beta_2$  in (36.2) in Ref. 26,

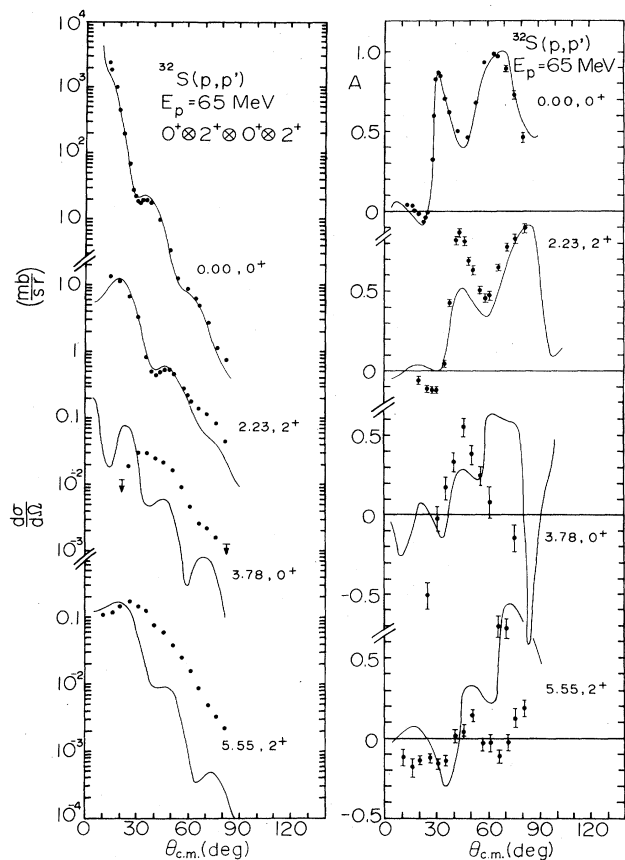


FIG. 19. Same as Fig. 18 except the 3.78,  $0^+$  and 5.55  $2^+$  states are assumed to belong to the  $\beta$  band and  $\eta_\beta R = 0.1$  fm

where  $I$  is the spin of any of the two-phonon states. The parameter  $\beta_{0I}''$  is essentially the  $\beta$  that appeared in (36.1) in Ref. 26. The direct coupling comes from an assumption that a nonvanishing amplitude of the one-phonon type of state is admixed into that of the two-phonon state. In the present calculations, the admixture was essential to reproduce the cross sections of the two-phonon states. The effect of the second order processes via the one phonon state was indeed negligible. The agreement between data and CC calculation is satisfactory for both cross sections and analyzing powers except for the  $0^+$ , 3.78 MeV state, where the fit is poor for both angular distributions.

A comparison between the CC calculation and the data is given in Fig. 24 for the coupling among the ground, one quadrupole phonon, and one octupole phonon states. The coupling parameters are  $\beta_{02} = 0.24$ ,  $\beta_{23} = 0.24$ , and  $\beta_{03} = 0.26$  in which the direct coupling between the ground and  $3^-$  states was essential. The  $\beta_{03}$  is just the  $\beta_3$  in (36.1) in Ref. 26. The fit to the  $3^-$  state is very good for the cross section, while it is not very good for the analyzing power.

#### IV. DISCUSSION

For  $^{12}\text{C}$ , the optical model could not reproduce the elastic cross section and analyzing power simultaneously.

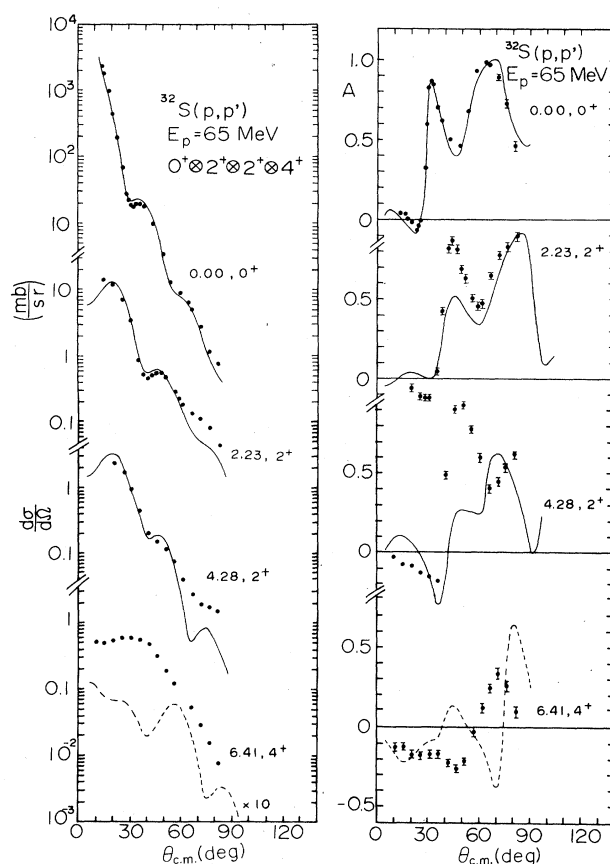


FIG. 20. Same as Fig. 18 except the 4.28,  $2^+$ ; 5.41,  $3^+$ ; and 6.41,  $4^+$  states are assumed to belong to the  $\gamma$  band and  $\eta_\gamma R = 0.48$  fm.

The fit to the data was unsatisfactory compared with that for heavier nuclei. However, the CC fit to the  $2^+$ , 4.44 MeV level is rather satisfactory for both angular distributions. This supports the idea that the  $^{12}\text{C}$  nucleus can naturally be treated as a deformed oblate nucleus. The rather fair fit to the data of the  $0^+$ , 7.66 MeV level in both the cross section and analyzing power supports the assignment of a  $\beta$ -vibrational band head to the  $0^+$  state.

The sign of  $\beta_2$  for the nuclei treated here could not be determined from the angular distributions of the  $2_1^+$  level alone. Generally a nucleus in which the head of the  $0^-$  octupole band is located at higher excitation than the octupole  $3^-$  band head is expected to have an oblate shape in the deformation of the ground band, and a nucleus in which the order of the  $3^-$  and  $0^-$  band heads is reversed has a prolate shape.<sup>38</sup> The signs adopted here are consistent with the expectation for  $^{24}\text{Mg}$  and  $^{28}\text{Si}$ . For  $^{12}\text{C}$  the  $1^-$  levels, the head of the  $K^\pi = 0^-$  band, is possibly identified as the 10.84 MeV state which is located at a higher excitation energy than the  $3^-$ , 9.64 MeV level. Then the sign of  $\beta_2$  should be negative and is consistent with the one adopted here.

While the cross sections for the  $2_1^+$  levels are well fitted by CC calculations using the rotational model for  $^{12}\text{C}$ ,  $^{24}\text{Mg}$ , and  $^{28}\text{Si}$  nuclei, the discrepancy between the data

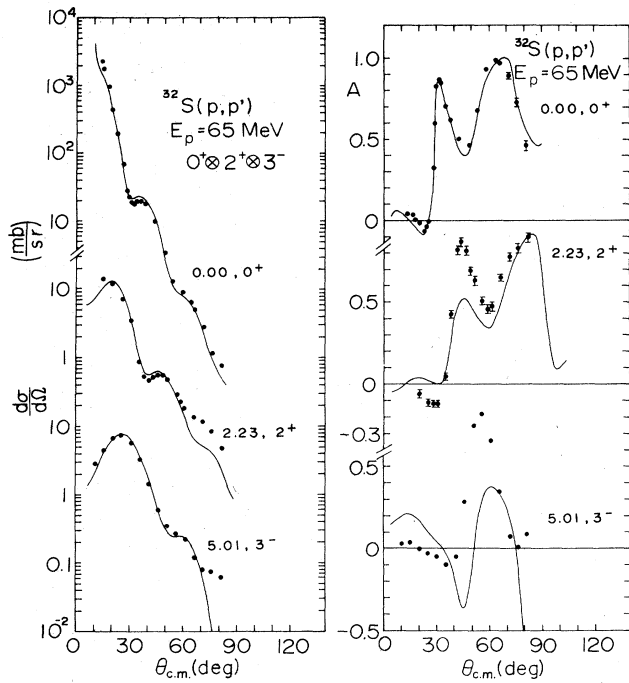


FIG. 21. Same as Fig. 18 except the 5.01,  $3^-$  state is assumed to belong to the octupole  $K^\pi=3^-$  vibrational band and  $\eta_3 R = 1.05$  fm.

and the CC curves are obvious for the  $4^+$  levels. This seems to be in contradiction with the very clear rotational spectrum of excitation energies of the ground bands in these nuclei. However, this is not the case. Excitation energies are related to diagonal components of interactions, whereas the differential cross sections are associated with a nondiagonal element of an interaction matrix. Therefore the cross section depends sensitively on a small admixture in the wave function of the final state. The small cross section for the  $4^+$  levels may be greatly affected by small components in the wave function besides the main rotational wave function. The value of  $\beta_4$  in Table II is thus tentative for 65 MeV. At 800 MeV incident energy, the fit is rather satisfactory for the cross section.<sup>14</sup>

For  $^{12}\text{C}$ ,  $^{24}\text{Mg}$ , and  $^{28}\text{Si}$ , the CC fits to the analyzing power data of the  $0_2^+$  levels are slightly improved by the mixing of the breathing oscillation to the  $\beta$  vibration. An unphysical dip at  $20^\circ$  or  $15^\circ$  in the CC predictions is re-

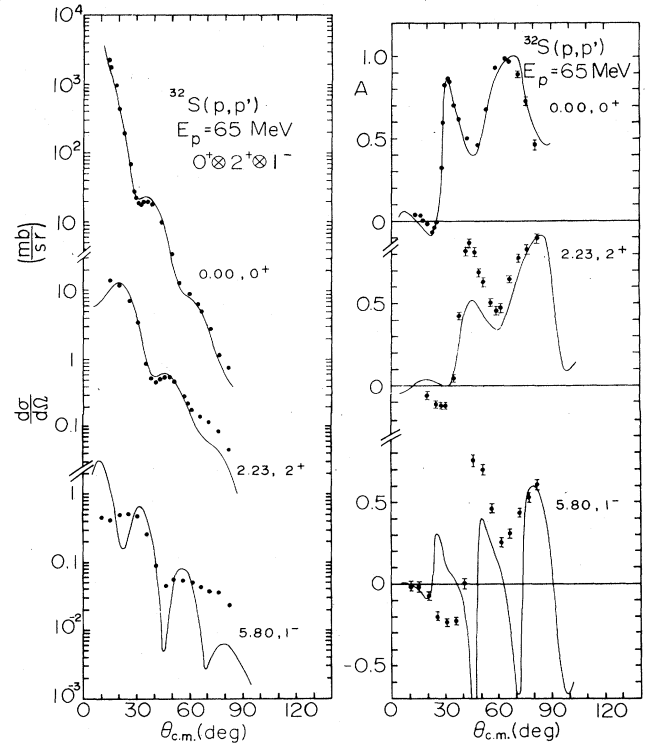


FIG. 22. Same as Fig. 18 except the 5.80,  $1^-$  state is assumed to belong to the octupole  $K^\pi=0^-$  vibrational band and  $\eta_0^- R = 1.5$  fm.

moved by the additional compressional oscillation. The sign of the breathing parameter  $\eta$  of the oscillation is ascertained to be the same as the sign of the deformation parameter  $\beta_2$  of the ground band. However, overall fits to the cross section are not improved appreciably by the mixing. The analyzing power is shown to be sensitive to the monopole oscillations. The improvement indicates the inclusion of the monopole breathing oscillation in the  $\beta$  vibration in these nuclei. The sign of  $\eta$  was uniquely determined but the magnitude was poorly determined by the CC calculation.

We calculated the CC curves for the  $4^-$ , 8.41;  $5^-$ , 9.70; and  $6^-$ , 11.58 MeV levels assuming them to be members of the  $3^-$  octupole vibrational band. However, the CC cross sections do not reach the experimental ones, as seen in Fig. 16. For the  $4^-$  level, the CC cross section is small-

TABLE II. Deformation length  $\beta R$  and coupling length  $\eta R$  of the excited states in  $^{12}\text{C}$  obtained in the coupled channels analysis with the symmetrical rotator model.

$E$ (MeV)	Particle	$\beta_2 R$ (fm)	$\beta_4 R$ (fm)	$\eta \beta R$ (fm)	$\eta_3 R$ (fm)	Ref.
30-40	(p,p')	-1.62	0.00			16
65	(p,p')	-1.82	0.17	1.48	0.94	This work
800	(p,p')	-1.91	0.002		1.21 <sup>a</sup>	13
183,250	(e,e')	-1.94 <sup>b</sup>	0.17 <sup>b</sup>			34

<sup>a</sup>Deduced from DWBA calculation.

<sup>b</sup>Typical values taken from Ref. 34.

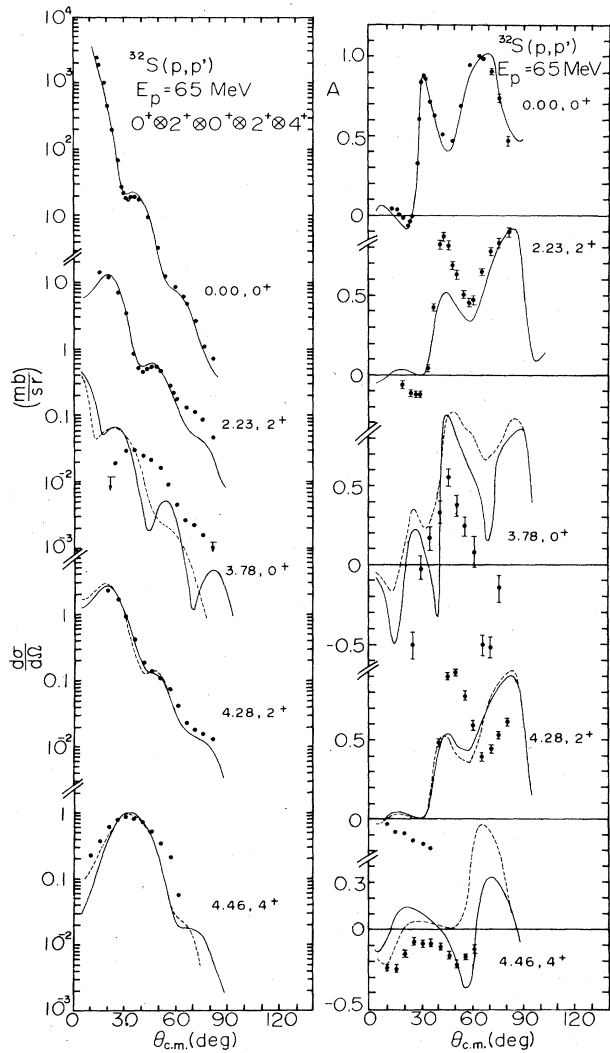


FIG. 23. Experimental angular distributions of the cross sections and analyzing powers and CC calculations for inelastic scattering on  $^{32}\text{S}$  by a vibrational model. This figure contains one quadrupole phonon state  $2^+$ , 2.23 MeV and three two-quadrupole phonon states  $0^+$ , 3.78;  $2^+$ , 4.28; and  $4^+$ , 4.64 besides the ground state. All states are coupled. The coupling parameters are  $\beta_{02}=0.24$ ,  $\beta_{20}=\beta_{22}=\beta_{24}=0.24$ ,  $\beta''_{00}=0.02$  (dashed curve),  $\beta''_{00}=-0.02$  (solid curve) for the  $0^+$  state;  $\beta''_{02}=0.12$  (dashed curve),  $\beta''_{02}=-0.12$  (solid curve) for the  $2^+$  state, and  $\beta''_{04}=0.12$  (dashed curve),  $\beta''_{04}=-0.11$  (solid curve). The meaning of the coupling parameters is explained in the text.

er by a factor of 5 than the data, for the  $5^-$  level smaller by a factor of 10, and for the  $6^-$  level smaller by a factor of  $10^3$ . Therefore the main component of the wave functions of these levels is not a collective one. They are alternatively thought to have a  $(1f_{7/2}1d_{5/2})$  particle-hole component in their structure.<sup>39</sup>

The deformation length  $\beta_\lambda R$  and the coupling length  $\eta_\lambda R$  are listed in Table III for  $^{24}\text{Mg}$  together with the values obtained from  $(p,p')$  scattering at various incident energies, other hadron scattering, and electron scattering. We did not take into account an asymmetric deformation

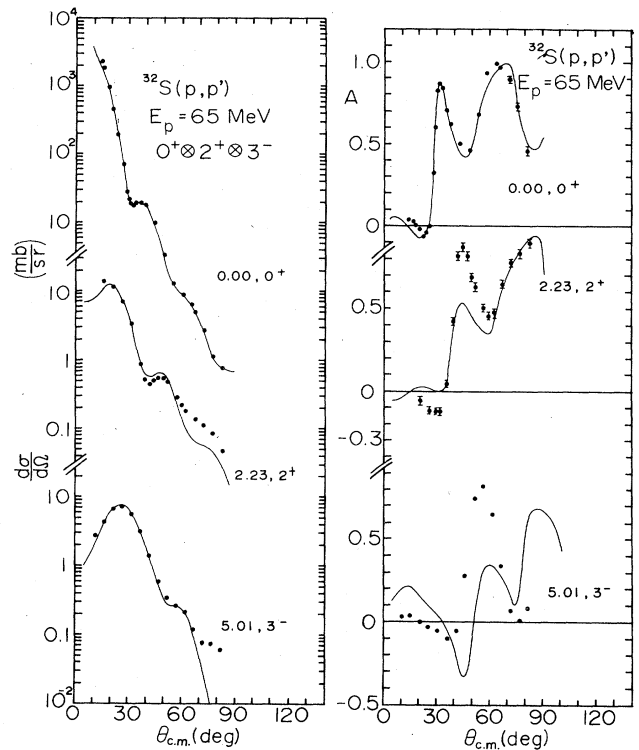


FIG. 24. Same as Fig. 23 except the ground state, one quadrupole phonon state  $2^+$ , 2.23 MeV, and one octupole phonon state  $3^-$ , 5.01 MeV are included. The coupling parameters are  $\beta_{02}=0.24$ ,  $\beta_{23}=0.26$ , and  $\beta''_{03}=0.26$ .

in this work. In our calculation, CC curves of the  $4^+$  state in the  $\gamma$  band did not agree with the data, as shown in Fig. 8. The vibrational operator  $\alpha_{42}$  may be essential to describe the level, as stated in Ref. 13. The values of the deformation length  $\beta_2 R$  extracted from hadron and electron scattering are well concentrated in a narrow band. The values of the coupling length  $\eta_\gamma R$  are also concentrated in a narrow range, whereas the values of  $\beta_4 R$  vary in a wide range. This is because the CC fit to the  $4^+$  data is not good in many cases. The CC fit to the  $4^+$ , 4.12 MeV level is generally comparable to that for the  $2^+$  level except for 800 MeV data.<sup>13</sup> The deformation length  $\beta R$  and the coupling length  $\eta R$  of the excited states in the  $^{28}\text{Si}$  obtained from hadron and electron scattering are listed in Table IV. The values of  $\beta_2 R$  for hadron scattering are well concentrated in a narrow range and are also close to the  $\beta_2 \langle R^2 \rangle^{1/2}$  value deduced from electron scattering. The values of  $\beta_4 R$  for  $(p,p')$  scattering are somewhat larger than the  $\beta_4 R$  value for  $(\alpha,\alpha')$  scattering or the  $\beta_4 \langle R^4 \rangle^{1/4}$  value for  $(e,e')$  scattering.

The good fit of the CC calculation to the  $\beta$ -vibrational states in  $^{24}\text{Mg}$  and  $^{28}\text{Si}$  for both cross section and analyzing power suggests that the CC calculation is suited for description and vibrational states of zero spin. We, however, obtained a very poor fit to the  $0^+$ , 3.78 MeV state in  $^{32}\text{S}$  assuming the state to be the head of a  $\beta$ -vibrational band. This shows that the  $0^+$  state does not belong to a  $\beta$

TABLE III. Deformation length  $\beta R$  and coupling length  $\eta R$  of the excited states in  $^{24}\text{Mg}$  obtained in the coupled channels analysis with the symmetrical rotator model and with the asymmetric rotator model in which the ground band is coupled to the  $\gamma$  band. The matrix elements  $\eta_{\gamma_1}R$  and  $\eta_{\gamma_2}R$  are explained in Ref. 6.

$E$ (MeV)	Particle	$\beta_2 R$ (fm)	$\beta_4 R$ (fm)	$\gamma$	$\eta_{\beta} R$ (fm)	$\eta_{\gamma_1} R$ (fm)	$\eta_{\gamma_2} R$ (fm)	$\eta_3 R$ (fm)	$\eta_0 - R$ (fm)	Ref.
17.5	(p,p')	1.65	-0.18							44
20.3	(p,p')	1.56	-0.19	21.5°		0.60	0.0			3
20.4	(p,p')	1.45	-0.08	21°		0.531	-0.235			8
30	(p,p')	1.72		23°						40
40	(p,p')	1.68	0.11			0.56	0.90	0.83		2
49.5	(p,p')	1.66	-0.06	21°		0.606	-0.235			4
65	(p,p')	1.58	-0.07		0.59°	0.56		0.86	0.59	This work
800	(p,p')	1.61	-0.05	20°		0.56	0.0			7
800	(p,p')	1.60	-0.081	15°	0.41	0.42	0.72	0.89	0.60	13
56	(d,d')	1.44								36
70	( $\alpha, \alpha'$ )	1.84	-0.33			0.58		0.93		41
104	( $\alpha, \alpha'$ )	1.36	-0.05							42
197,250	(e,e')	1.36 <sup>a</sup>	-0.19 <sup>b</sup>							43

<sup>a</sup> $\beta_2 \langle R^2 \rangle^{1/2}$ .

<sup>b</sup> $\beta_4 \langle R^4 \rangle^{1/4}$ .

<sup>c</sup>Without breathing mode.

band of a deformed nucleus. The value of the cross section of the state is one order smaller compared with the corresponding states in  $^{24}\text{Mg}$  or  $^{28}\text{Si}$ . This may suggest that the state has a noncollective nature. The  $2^+$ , 4.28 MeV state in  $^{32}\text{S}$  is well fitted by assuming it to be a  $\gamma$ -vibrational state as illustrated in Fig. 20. (See also Table V.) Overall,  $^{32}\text{S}(p,p')$  scattering to various levels is explained by the deformed model of a nucleus as well as in the cases of the  $^{24}\text{Mg}(p,p')$  or  $^{28}\text{Si}(p,p')$  scattering except for the  $0_2^+$  level.

Alternatively we tried to fit the data by the vibrational model of a spherical nucleus. There are no appreciable differences in the CC results between the rotational and the vibrational model. The  $0^+$ , 3.78 MeV state is still not satisfactorily interpreted by assuming it to be a two-phonon state.

For nuclei treated here, the optical potentials are deformed and the deformation parameters are determined to fit the elastic and inelastic scattering data in the channel coupling approach. Assuming the folding model for the optical potential and using Satchler's theorem,<sup>17</sup> the mul-

tipole moments of the matter distribution<sup>47</sup> are obtained from those of the optical potential. Satchler's theorem states that the  $E\lambda$  multipole moment of the folding optical potential is equal to the  $E\lambda$  moment of the matter distribution. The multipole moments  $M(E\lambda)$  of the deformed optical potential  $V(r, \theta)$  are defined as<sup>48</sup>

$$M(E\lambda) = \frac{Ze \int r^\lambda Y_{\lambda 0}(\Omega') V(r, \theta') r^2 dr d\Omega'}{\int V(r, \theta') r^2 dr d\Omega'} \quad (5)$$

$$V(r, \theta') = \frac{V}{1 + \exp \left[ \left\{ r - r_R A^{1/3} \left[ 1 + \sum \beta_\lambda Y_{\lambda 0}(\theta') \right] / a \right\} \right]} \quad (6)$$

in which an axial symmetry of the potential is assumed in the body fixed coordinate system. This is the quantity which is related to the multipole moment of matter distribution and is compared directly with the charge distribution moment deduced from electromagnetic measurement. The values are shown in Table VI. The values agree well with each other except the  $M(E2)$  value for  $^{12}\text{C}$ , where

TABLE IV. Deformation length  $\beta R$  and coupling length  $\eta R$  of the excited states in  $^{28}\text{Si}$  obtained in the coupled channels analysis with the symmetric rotator model.

$E$ (MeV)	Particle	$\beta_2 R$ (fm)	$\beta_4 R$ (fm)	$\eta_{\beta} R$ (fm)	$\eta_3 R$ (fm)	Ref.
17.5	(p,p')	-1.28	+0.94			44
25-40	(p,p')	-1.31	+0.57		1.07	4
65	(p,p')	-1.17	+0.45	0.79°	0.75	This work
56	(d,d')	-1.18				36
104	( $\alpha, \alpha'$ )	-1.25	+0.30			42,45
187,250	(e,e')	-1.22 <sup>a</sup>	+0.34 <sup>b</sup>			43

<sup>a</sup> $\beta_2 \langle R^2 \rangle^{1/2}$ .

<sup>b</sup> $\beta_4 \langle R^4 \rangle^{1/4}$ .

<sup>c</sup>Without breathing mode.

TABLE V. Deformation length  $\beta R$  and coupling length  $\eta R$  of the excited states in  $^{32}\text{S}$  obtained in the coupling channels analysis with the symmetric rotator model and with the asymmetric rotator model in which the ground band is coupled to the  $\gamma$  band. The matrix elements  $\eta_{\gamma_1}R$  and  $\eta_{\gamma_2}R$  are explained in Ref. 6.

$E$ (MeV)	Particle	$\beta_2 R$ (fm)	$\beta_4 R$ (fm)	$\gamma$	$\eta_{\gamma_1} R$ (fm)	$\eta_{\gamma_2} R$ (fm)	$\eta_3 R$ (fm)	Ref.
17.5	(p,p')	-1.15	0.96					41
20.4	(p,p')	0.86	-0.88	33°	0.325	-0.125		8
65	(p,p')	0.95	-0.46		0.46		0.91	This work

the value extracted from present (p,p') data is larger than that from (e,e') data. For  $4^+$  levels in the ground band, the fit between the experimental cross sections and the CC calculations is generally not good for low incident energies. The values of  $M(E4)$  extracted from present 65 MeV (p,p') data are thus ambiguous for  $^{12}\text{C}$  and  $^{24}\text{Mg}$ .

In the excitation of the ground rotational band or the vibrational states, the transition strengths  $B(E\lambda)$  for the transition from spin  $\lambda$  state to the ground state are represented in units of their single particle value  $B(E\lambda)_{s.p.}$  as

$$\frac{B(E\lambda)}{B(E\lambda)_{s.p.}} = \frac{(3+\lambda)^2}{4\pi(2\lambda+1)} (Z\beta_\lambda^m)^2, \quad (7)$$

where  $\beta_\lambda^m$  is obtained<sup>49</sup> from

$$\beta_\lambda r_R = \beta_\lambda^m r_m, \quad r_m = 1.2 \text{ fm}.$$

Here  $\beta$  stands for deformation parameter  $\beta$  or coupling parameter  $\eta$  and  $Z$  is the atomic number. Transition strengths obtained are compared with the gamma-transition width  $\Gamma_\gamma(E\lambda)$  of the corresponding transition<sup>50</sup> represented in their Weisskopf unit  $\Gamma_W(E\lambda)$ . The comparison is given in Table VII for  $E2$  transitions in the

ground band. The table shows that the values obtained from the present analysis of (p,p') scattering are smaller than the corresponding values deduced from the gamma-transition rate except for the  $2_1^+$  to the ground state transition in  $^{12}\text{C}$ . This discrepancy, seen in the case of  $^{12}\text{C}$ , is consistent with the large value of the multipole moment derived from (p,p') scattering compared to that of (e,e') scattering as shown in Table VI. The larger values of the transition strength of hadron scattering over the gamma-transition widths in Table VII may be attributed to the diffuseness of the nuclear surface.<sup>51</sup> The relation (7) is derived from an assumption of a sharp cutoff picture of the nuclear surface.

## V. SUMMARY AND CONCLUSIONS

Angular distributions of the cross sections and analyzing powers for 65 MeV proton elastic and inelastic scattering to excited states in the ground band,  $\beta$  and  $\gamma$  bands, and octupole bands in the light even-even nuclei  $^{12}\text{C}$ ,  $^{24}\text{Mg}$ ,  $^{28}\text{Si}$ , and  $^{32}\text{S}$  have been presented. Coupled channels calculations assuming the collective rotational model provide a reasonable description of the data for  $2^+$  states of the ground state rotational bands. This shows the applicability of this model to these nuclei. Then the

TABLE VI. Multipole moments deduced from an optical potential and a charge density for deformed nuclei.

Nucleus	$M(E2)$ (eb)	$M(E4)$ (eb <sup>2</sup> )	Reaction	Ref.
$^{12}\text{C}$	-0.098	0.0076	65 MeV (p,p')	This work
	-0.0552	0.0019	800 MeV (p,p')	14
	-0.0643	0.0022	183,250 MeV (e,e')	34
$^{24}\text{Mg}$	0.230	0.011	65 MeV (p,p')	This work
	0.216	0.0073	20 MeV (p,p')	3
	0.204-0.276	0.007-0.019	23-29 MeV (p,p')	8,46
	0.245	0.0152	30 MeV (p,p')	40
	0.242-0.253	0.010-0.020	40 MeV (p,p')	2
	0.216-0.238	0.0083-0.0128	50 MeV (p,p')	8,48
	0.188	0.0073	800 MeV (p,p')	3
	0.224		56 MeV (d,d')	53
	0.209	0.0086	104 MeV ( $\alpha, \alpha'$ )	42
0.218±0.010	0.0041±0.0013	183,250 MeV (e,e')	43	
0.205±0.006	0.0073	Coulomb excitation	48	
$^{28}\text{Si}$	-0.155	-0.011	65 MeV (p,p')	This work
	-0.195		56 MeV (d,d')	36
	-0.202		183,250 MeV (e,e')	43
$^{32}\text{S}$	0.19	-0.029	65 MeV (p,p')	This work

TABLE VII. Transition strength  $B(E2)$  of hadron scattering in units of the single particle value  $B(E2)_{s.p.}$  and gamma transition widths  $\Gamma_\gamma(E2)$  in the Weisskopf unit  $\Gamma_W(E2)$  for  $E2$  transitions in the ground band.

Nucleus	Deformation	$\frac{B(E2)}{B(E2)_{s.p.}}$	$\frac{\Gamma_\gamma(E2)}{\Gamma_W(E2)}$
	parameter		
$^{12}\text{C}$	-0.64	6.3	$4.7 \pm 0.3^a$
$^{24}\text{Mg}$	0.48	11.9	$20 \pm 0.4^b$
$^{28}\text{Si}$	-0.34	8.0	$12.6 \pm 0.4^b$
$^{32}\text{S}$	0.25	6.4	$9.8 \pm 0.4^b$

<sup>a</sup>Reference 12.

<sup>b</sup>Reference 13.

CC calculation was extended to the states which were members of vibrational bands of these deformed nuclei. The excited  $0^+$  states of  $^{12}\text{C}$ ,  $^{24}\text{Mg}$ , and  $^{28}\text{Si}$  were well explained in both cross section and analyzing power assuming these states to be band heads of the  $\beta$  band. The fit to the analyzing power was improved by the additional mixing of the breathing oscillation in the  $\beta$  vibration. The  $\gamma$ -vibrational bands in  $^{24}\text{Mg}$  and  $^{32}\text{S}$  are well fitted by CC calculations only for the band head  $2^+$  states. The CC cross section was smaller than the experimental cross section for the higher states in the  $\gamma$  bands. The CC cross section produced only  $\frac{1}{100}$  of the strength of the  $3^+$  level and  $\frac{1}{10}$  of the strength of the  $4^+$  level in the  $\gamma$  band of  $^{24}\text{Mg}$ . Octupole vibrational bands are observed in all nuclei concerned. For the  $3^-$ , 7.62 MeV in  $^{24}\text{Mg}$ , an agreement between the CC curves and the data was good. The  $3^-$  levels of the  $3^-$  band head in  $^{12}\text{C}$ ,  $^{24}\text{Mg}$ , and  $^{28}\text{Si}$  were explained by the macroscopic calculation though the CC fit was not always satisfactory. The  $4^-$ ,  $5^-$ , and  $6^-$  states in  $^{28}\text{Si}$  were not explained by the CC calculation, which could not produce the rather large experimental cross sections of these levels. The  $3^-$  state in  $^{32}\text{S}$  was very well reproduced for the cross section but not for the analyzing power. The band head  $1^-$  states of  $K^\pi=0^-$  octupole bands in  $^{24}\text{Mg}$  and  $^{28}\text{Si}$  could not be fitted by CC curves in both cross section and analyzing power, while the  $3^-$

states belonging to the band were reasonably fitted by CC curves. The CC calculations assuming the vibrational model of spherical nuclei were performed only for  $^{32}\text{S}$ .  $^{32}\text{S}$  has been equally well described by both the rotational and vibrational models.

Deformation lengths and coupling lengths of the excited states were extracted from the CC calculations. They agreed reasonably well with those extracted from scattering with different energies and particles and also electromagnetic measurements. Using the deformation lengths  $\beta_2 R$  and  $\beta_4 R$  of the ground rotational band, multipole moments of the deformed optical potentials are derived. The moments were related to those of the deformed matter densities by Satchler's theorem and compared to the values obtained with other hadronic probes and to the multipole moments of the charge density obtained via electromagnetic measurements. They agree well within their errors, though the errors were difficult to assess.

The transition strengths from the ground band states or vibrational states to the ground state were obtained. They were compared with the gamma-ray transition width of corresponding transitions. The values of the transition strengths of (p,p') scattering were smaller than the corresponding value of the gamma transition width. This fact may be explained by the surface diffuseness of the nucleus, which was not taken into account in the calculation of the transition strengths.

#### ACKNOWLEDGMENTS

The authors would like to thank the cyclotron crew for operation of the cyclotron. The authors are grateful to the late Professor S. Yamabe for his continuous advice and encouragement in the early stages of this work. We would like to acknowledge Dr. M. Nomura at the University of Tokyo for his ingenious discussions on the levels in octupole bands. The authors are also indebted to Dr. M. Fujiwara at RCNP who kindly instructed us in the peak fitting procedure in the spectrum analyses. This experiment was performed at the Research Center for Nuclear Physics, Osaka University, under Program Nos. 3A17, 4A2, and 14A2.

<sup>1</sup>A. G. Blair, C. Glashauser, R. De Swiniarski, J. Goudergues, R. Lombard, B. Mayer, J. Thirion, and P. Vaganov, Phys. Rev. C **1**, 444 (1970).

<sup>2</sup>B. Zwieglinski, G. M. Crawley, H. Nann, and J. A. Nolen, Jr., Phys. Rev. C **17**, 872 (1978); B. Zwieglinski, G. M. Crawley, W. Chung, H. Nann, and J. A. Nolen, Jr., *ibid.* **18**, 1228 (1978).

<sup>3</sup>R. M. Lombard, J. L. Escudié, and M. Soyeur, Phys. Rev. C **18**, 42 (1978).

<sup>4</sup>R. De Leo, G. D'Erasmus, A. Pantaleo, G. Pasquariello, G. Viesti, M. Pignanelli, and H. V. Geramb, Phys. Rev. C **19**, 646 (1979).

<sup>5</sup>R. De Leo, G. D'Erasmus, E. M. Fiore, A. Pantaleo, M. Pignanelli, and H. V. Geramb, Phys. Rev. C **20**, 13 (1979).

<sup>6</sup>L. Ray, G. S. Blanpied, and W. R. Coker, Phys. Rev. C **20**, 1236 (1979).

<sup>7</sup>G. S. Blanpied, N. M. Hintz, G. S. Kyle, J. W. Palm, R. Liljestrand, M. Barlett, C. Harvey, G. W. Hoffmann, L. Ray, and D. G. Madland, Phys. Rev. C **20**, 1490 (1979).

<sup>8</sup>R. De Leo, G. D'Erasmus, A. Pantaleo, M. N. Harakeh, S. Micheletti, and M. Pignanelli, Phys. Rev. C **23**, 1355 (1981).

<sup>9</sup>D. K. Hasell, N. E. Davison, T. N. Nasr, B. T. Murdoch, A. M. Sourkes, and W. T. H. van Oers, Phys. Rev. C **27**, 482 (1983).

<sup>10</sup>J. D. Garrett, H. T. Fortune, R. Middleton, and W. Scholz, Phys. Rev. C **18**, 2032 (1978).

<sup>11</sup>J. L. C. Ford, Jr. *et al.*, Phys. Rev. C **21**, 764 (1980).

<sup>12</sup>F. Ajzenberg-Selove and C. L. Busch, Nucl. Phys. **A336**, 1 (1980).

<sup>13</sup>G. S. Blanpied *et al.*, Phys. Rev. C **25**, 422 (1982).

<sup>14</sup>G. S. Blanpied *et al.*, Phys. Rev. C **23**, 2599 (1981).

<sup>15</sup>M. N. Harakeh and R. De Leo, Phys. Lett. **117B**, 377 (1982).

- <sup>16</sup>R. De Leo, G. D'Erasmus, A. Pantaleo, M. N. Harakeh, E. Cereda, S. Micheletti, and M. Pignanelli, *Phys. Rev. C* **28**, 1443 (1983).
- <sup>17</sup>G. R. Satchler, *J. Math. Phys.* **13**, 1113 (1972).
- <sup>18</sup>K. Imai, N. Tamura, and K. Nisimura, Research Center for Nuclear Physics Annual Report, 1976, p. 23.
- <sup>19</sup>M. Nakamura, *et al.*, *J. Phys. Soc. Jpn. Suppl.* **44**, 41 (1978).
- <sup>20</sup>N. Matsuoka, K. Hosono, T. Saito, A. Shimizu, and M. Kondo, Research Center for Nuclear Physics Annual Report, 1976, p. 97.
- <sup>21</sup>K. Hosono, M. Kondo, T. Saito, N. Matsuoka, S. Nagamachi, S. Kato, K. Ogino, Y. Kadota, and T. Noro, *Phys. Rev. Lett.* **41**, 621 (1978).
- <sup>22</sup>H. Ikegami, S. Morinobu, I. Katayama, M. Fujiwara, and S. Yamabe, *Nucl. Instrum. Methods* **175**, 335 (1980).
- <sup>23</sup>K. Imai, K. Hatanaka, H. Shimizu, and K. Nisimura, Research Center for Nuclear Physics Annual Report, 1978, p. 154.
- <sup>24</sup>Y. Fujita, K. Nagayama, S. Morimobu, M. Fujiwara, I. Katayama, T. Yamazaki, and H. Ikegami, *Nucl. Instrum. Methods* **173**, 265 (1980).
- <sup>25</sup>M. Nakamura, private communication.
- <sup>26</sup>T. Tamura, *Rev. Mod. Phys.* **37**, 679 (1965).
- <sup>27</sup>T. Tamura, Oak Ridge National Laboratory Report No. ORNL-4152, 1967 (unpublished).
- <sup>28</sup>M. P. Fricke, R. M. Drisco, R. H. Bassel, E. E. Gross, B. J. Morton, and A. Zucker, *Phys. Rev.* **163**, 1153 (1967).
- <sup>29</sup>T. Wada, The Institute of Physical and Chemical Research, code SEARCH.
- <sup>30</sup>J. Raynal, Saclay, code MAGALI.
- <sup>31</sup>A. Bohr and B. R. Mottelson, *Nuclear Structure* (Benjamin, Reading, Mass., 1975), Vol. II, Fig. 6-3, p. 363.
- <sup>32</sup>G. R. Satchler, *Part. Nucl.* **5**, 105 (1973).
- <sup>33</sup>B. J. Verhaar, W. C. Hermans, and J. Oberski, *Nucl. Phys.* **A195**, 379 (1972).
- <sup>34</sup>A. Nakada, Y. Torizuka, and Y. Horikawa, *Phys. Rev. Lett.* **27**, 745 (1971).
- <sup>35</sup>A. Christy and O. Häusser, *Nucl. Data Tables* **11**, 281 (1972).
- <sup>36</sup>K. Hatanaka, M. Nakamura, K. Imai, T. Noro, H. Shimizu, H. Sakamoto, J. Shirai, T. Matsuse, and K. Nisimura, *Phys. Rev. Lett.* **46**, 15 (1981).
- <sup>37</sup>T. Tamura, *Prog. Theor. Phys. Suppl. No.* **37–38**, 383 (1966).
- <sup>38</sup>M. Nomura, *Phys. Lett.* **55B**, 357 (1975).
- <sup>39</sup>K. Hosono, N. Matsuoka, K. Hatanaka, T. Saito, T. Noro, M. Kondo, S. Kato, K. Okada, K. Ogino, and Y. Kadota, *Phys. Rev. C* **26**, 1440 (1982).
- <sup>40</sup>J. Eenmaa, R. K. Cole, C. N. Waddell, H. S. Sandhu, and R. R. Dittman, *Nucl. Phys.* **A218**, 125 (1974).
- <sup>41</sup>G. C. Yang, P. P. Singh, A. van der Woude, and A. G. Drentje, *Phys. Rev. C* **13**, 1376 (1976).
- <sup>42</sup>H. Rebal, G. W. Schweimer, G. Schatz, J. Specht, R. Löhken, G. Hauser, D. Habs, and H. Klewe-Nebenius, *Nucl. Phys.* **A182**, 145 (1972).
- <sup>43</sup>Y. Horikawa, Y. Torizuka, A. Nakada, S. Mitsunobu, Y. Kojima, and M. Kimura, *Phys. Lett.* **36B**, 9 (1971).
- <sup>44</sup>R. de Swiniarski, C. Glashausser, D. L. Hendrie, J. Sherman, A. D. Bacher, and E. A. McClatchie, *Phys. Rev. Lett.* **23**, 317 (1964).
- <sup>45</sup>H. Rebel, G. W. Schweimer, J. Specht, G. Schatz, R. Löhken, D. Habs, G. Hauser, and H. Klewe-Nebenius, *Phys. Rev. Lett.* **26**, 1190 (1971).
- <sup>46</sup>I. Lovas, M. Rogge, U. Schwinn, P. Turek, D. Ingham, and C. Mayer-Böricke, *Nucl. Phys.* **A286**, 12 (1977).
- <sup>47</sup>R. M. Ronningen, J. H. Hamilton, L. Varnell, J. Lange, A. V. Ramayya, G. Garcia-Bermudez, W. Lourens, L. L. Riedinger, F. K. McGowan, P. H. Stelson, R. L. Robinson, and J. L. C. Ford, Jr., *Phys. Rev. C* **16**, 2208 (1977).
- <sup>48</sup>R. S. Mackintosh, *Nucl. Phys.* **A266**, 379 (1976).
- <sup>49</sup>A. M. Bernstein, V. R. Brown, and V. A. Madsen, *Phys. Rev. Lett.* **42**, 425 (1979); *Phys. Lett.* **103B**, 255 (1981).
- <sup>50</sup>P. M. Endt and C. van der Leun, *At. Data Nucl. Data Tables* **13**, 67 (1974).
- <sup>51</sup>A. M. Bernstein, in *Advances in Nuclear Physics*, edited by M. Beranger and E. Vogt (Plenum, New York, 1969), Vol. 3, p. 325.
- <sup>52</sup>P. M. Endt and C. van der Leun, *Nucl. Phys.* **A310**, 1 (1978).
- <sup>53</sup>K. Hatanaka, N. Matsuoka, T. Saito, K. Hosono, M. Kondo, S. Kato, T. Higo, S. Matsuki, and K. Ogino, *Nucl. Phys.* **A403**, 109 (1983).